Geosci. Model Dev., 5, 149–166, 2012
www.geosci-model-dev.net/5/149/2012/
doi:10.5194/gmd-5-149-2012

Geoscientific Model Development

LOSCAR: Long-term Ocean-atmosphere-Sediment CArbon cycle Reservoir Model v2.0.4

R. E. Zeebe

School of Ocean and Earth Science and Technology, University of Hawaii at Manoa, 1000 Pope Road, MSB 504, Honolulu, 96822, USA

Correspondence to: R. E. Zeebe (zeebe@soest.hawaii.edu)

Received: 24 May 2011 – Published in Geosci. Model Dev. Discuss.: 29 June 2011
Revised: 12 January 2012 – Accepted: 18 January 2012 – Published: 25 January 2012

Abstract. The LOSCAR model is designed to efficiently compute the partitioning of carbon between ocean, atmosphere, and sediments on time scales ranging from centuries to millions of years. While a variety of computationally inexpensive carbon cycle models are already available, many are missing a critical sediment component, which is indispensable for long-term integrations. One of LOSCAR's strengths is the coupling of ocean-atmosphere routines to a computationally efficient sediment module. This allows, for instance, adequate computation of $CaCO_3$ dissolution, calcite compensation, and long-term carbon cycle fluxes, including weathering of carbonate and silicate rocks. The ocean component includes various biogeochemical tracers such as total carbon, alkalinity, phosphate, oxygen, and stable carbon isotopes. LOSCAR's configuration of ocean geometry is flexible and allows for easy switching between modern and paleo-versions. We have previously published applications of the model tackling future projections of ocean chemistry and weathering, $p\mathrm{CO_2}$ sensitivity to carbon cycle perturbations throughout the Cenozoic, and carbon/calcium cycling during the Paleocene-Eocene Thermal Maximum. The focus of the present contribution is the detailed description of the model including numerical architecture, processes and parameterizations, tuning, and examples of input and output. Typical CPU integration times of LOSCAR are of order seconds for several thousand model years on current standard desktop machines. The LOSCAR source code in C can be obtained from the author by sending a request to loscar.model@gmail.com.

1 Introduction

Various carbon cycle models that are computationally inexpensive have been developed in the past, in particular box models of the ocean's carbon cycle (e.g. Sarmiento and Toggweiler, 1984; Siegenthaler and Wenk, 1984; Walker and Kasting, 1992; Toggweiler, 1999; Stephens and Keeling, 2000; Köhler et al., 2005; Peacock et al., 2006). However, less studies have coupled a genuine sediment model to the ocean box model (e.g. Sundquist, 1986; Keir, 1988; Opdyke and Walker, 1992; Sigman et al., 1998; Ridgwell, 2001) and also considered long-term carbon cycle fluxes and feedbacks such as carbonate and silicate rock weathering (e.g. Munhoven and Francois, 1996; Shaffer et al., 2008). The LOSCAR model (Long-term Ocean-atmosphere-Sediment CArbon cycle Reservoir model) closes this gap. In addition, LOSCAR's configuration of ocean geometry is flexible (cf. Ridgwell, 2001) and allows for easy switching between modern and paleo-versions (see below). Note also that LOSCAR's sediment module includes variable porosity (Sect. 6.2). LOSCAR is primarily designed to efficiently compute the partitioning of carbon between ocean, atmosphere, and sediments on time scales ranging from centuries to millions of years. LOSCAR includes various biogeochemical tracers such as total dissolved inorganic carbon (TCO_2), total alkalinity (TA), phosphate (PO_4), oxygen (O_2), stable carbon isotopes (δ^{13}C), and %$CaCO_3$ in sediments. Based on the predicted tracer distributions, different variables are computed including atmospheric CO_2, ocean pH, calcite and aragonite saturation state, calcite compensation depth (CCD) and more. LOSCAR also allows for changes in the major ion composition of seawater, including the seawater Mg/Ca ratio, which is critical for paleo-applications. The major ion seawater composition affects thermodynamic quantities such as equilibrium constants and solubility products, which in turn affect the predicted ocean carbonate chemistry and atmospheric CO_2.

We have previously published several applications of LOSCAR dealing, for instance, with future projections of ocean chemistry and weathering, pCO$_2$ sensitivity to carbon cycle perturbations throughout the Cenozoic, and carbon/calcium cycling during the Paleocene-Eocene Thermal Maximum (PETM) (Zeebe et al., 2008; Zachos et al., 2008; Zeebe et al., 2009; Uchikawa and Zeebe, 2008; Stuecker and Zeebe, 2010; Uchikawa and Zeebe, 2010; Komar and Zeebe, 2011; Zeebe and Ridgwell, 2011; Zeebe, 2012). The subject of the present contribution is the detailed description of the model including numerical architecture, processes and parameterizations, tuning, and examples of input and output. It may appear that publishing model applications before a detailed model description is putting the cart before the horse. One of the reasons for this is that the journals interested in publishing the model applications have little or no interest in publishing a detailed model description. Journals that provide a forum for technical model descriptions are rare, and so the recent appearance of *Geoscientific Model Development* has encouraged me to provide a coherent model description of LOSCAR that will hopefully be useful for the readership of the journal, as well as the users of the model. On the other hand, publishing a few model applications before the detailed model description also has an advantage. LOSCAR, for example, has been extensively tested by now and several minor bugs and numerical issues have already been fixed (see Sect. 7.4).

LOSCAR's main components include ocean, atmosphere, and marine sediments. The model architecture, main components, model variables, and process parameterizations will be described in the following. Finally, two input/output examples will be presented, one dealing with anthropogenic fossil fuel emissions, the other with carbon release during the PETM (input files for these examples are included in the model package).

2 Architecture

The basic numerical architecture of the model is fairly simple. For all model variables y_i, i.e. all tracers in all compartments (atmosphere, ocean boxes, and sediment boxes), a system of coupled, first-order ordinary differential equations is solved:

$$\frac{\mathrm{d}y_i}{\mathrm{d}t} = F(t, y_1, y_2, \ldots, y_{\mathrm{NEQ}}) , \tag{1}$$

where t is time, NEQ is the total number of equations, $i = 1, 2, \ldots, \mathrm{NEQ}$, and F's are known functions. Note that for most applications, the derivatives (right-hand side of Eq. 1) do not explicitly depend on the independent variable t. For given start (initial) conditions $\boldsymbol{y}_0$ at t_{start}, the equations are then integrated forward in time over the interval from t_{start} to t_{final}. Standard numerical procedures (solvers) for this sort of problem are available. One thing to keep in mind is that the equations solved in LOSCAR are typically stiff and involve different time scales, which requires a solver for stiff problems with adaptive stepsize control. The solver implemented in the C version of LOSCAR is a fourth-order Rosenbrock method with automatic stepsize adjustment (Press et al., 1992).

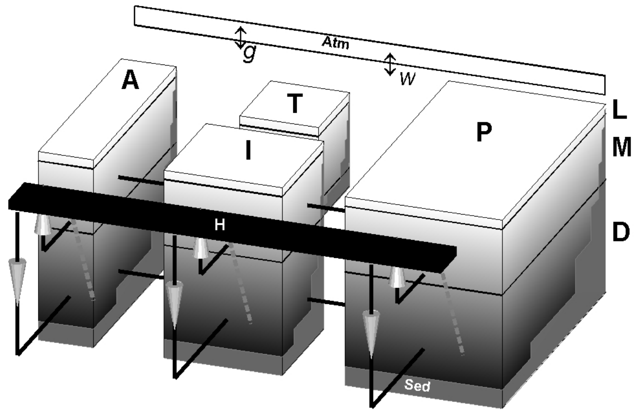

Fig. 1. Schematic representation of the LOSCAR model (Paleocene/Eocene configuration). A = Atlantic, I = Indian, P = Pacific, T = Tethys ocean, H = High-latitude surface, L = Low-latitude surface, M = interMediate, D = Deep box. Weathering fluxes and gas exchange with the atmosphere (Atm) are indicated by "w" and "g", respectively. Steps on the faces of ocean boxes indicate sediments (Sed).

Once the initial conditions $\boldsymbol{y}_0$ and derivatives F's have been supplied, the solution of the problem is usually straightforward. However, setting up $\boldsymbol{y}_0$ and F requires some work. In the following, the individual model components will be described and expressions will be given for individual F's that enter Eq. (1). The current setup includes two different model versions: a "modern" version and a Paleocene/Eocene version ("P/E"-version for short).

3 Ocean

3.1 Geometry

The global ocean is geometrically divided in LOSCAR into separate ocean basins representing Atlantic, Indian, and Pacific Ocean (plus Tethys in the P/E-version). In turn, each ocean basin is subdivided into surface, intermediate, and deep ocean (Fig. 1). In addition, the model includes a generic high-latitude box (H-box), representing cold surface waters without reference to a specific location (cf. Walker and Kasting, 1992; Toggweiler, 1999). As a result, the total number of ocean boxes is NB = 10 in the modern version and NB = 13

Table 1. Model-architecture and ocean geometry parameters.

Parameter	Symbol	Value[a]	Unit
# Ocean basins	NOC	3 (4)	–
# Ocean tracers	NOCT	varies	–
# Ocean boxes	NB	10 (13)	–
# Atm. tracers	NATM	1 or 2[b]	–
# Sediment levels	NSD	13	–
# Equations	NEQ	NOCT × NB + NATM + NOC × NSD	–
Total ocean volume	V_{oc}	$1.29\times10^{18,c}$	m^3
Total ocean area	A_{oc}	$3.49\times10^{14,c}$	m^2
% Area	f_A	26,18,46,10[d]	%
% Area	f_A	(15,14,52,9,10)[e,f]	%
Height L-box[g]	h_L	100	m
Height H-box[g]	h_H	250	m
Height M-box[g]	h_M	900	m
Volume M-boxes[g]	V_i	0.817, 0.565, 1.445[h]	$10^{17}m^3$
Volume M-boxes[g]	V_i	(0.471, 0.440, 1.633, 0.283)[j]	$10^{17}m^3$
Volume D-boxes[g]	V_i	2.853, 2.099, 4.739[h]	$10^{17}m^3$
Volume D-boxes[g]	V_i	(1.540, 1.540, 6.547, 0.063)[j]	$10^{17}m^3$

[a] Default: modern version, parentheses: P/E-version. [b] 1: CO_2 ; 2: CO_2 and $^{13}CO_2$. [c] Toggweiler (1999). [d] Atlantic, Indian, Pacific, High-latitude. [e] (Atlantic, Indian, Pacific, Tethys, High-latitude). [f] Bice and Marotzke (2002). [g] L = Low-latitude surface, H = High-latitude surface, M = interMediate, D = Deep. [h] Atlantic, Indian, Pacific. [j] (Atlantic, Indian, Pacific, Tethys).

in the P/E-version. Box areas and volumes are given in Table 1. The modern ocean geometry in LOSCAR is not unlike the one used by Walker and Kasting (1992). However, Walker and Kasting (1992) combined the warm surface and thermocline waters each into a single reservoir for a total of 6 boxes to represent the global modern ocean.

The modern and Paleocene/Eocene ocean bathymetry in LOSCAR is based on Menard and Smith (1966) and Bice and Marotzke (2002), respectively. The bathymetry determines the surface area and volume of ocean boxes (Table 1) and the surface area-depth level relationship of the sediment boxes (Sect. 6).

3.2 Ocean tracer equations

Let y_k be a subset of $\boldsymbol{y}$ (Eq. 1), representing ocean tracer variables including TCO_2, TA, PO_4, etc. (in this particular order). Then $k = 1, 2, \ldots, \mathrm{NB}$ for TCO_2, $k = \mathrm{NB}+1, \mathrm{NB}+2, \ldots, 2\,\mathrm{NB}$ for TA, $k = 2\,\mathrm{NB}+1, 2\,\mathrm{NB}+2, \ldots, 3\,\mathrm{NB}$ for PO_4, and so on. If the total number of ocean tracers is NOCT, then the total number of equations for all ocean tracers and boxes is NOCT × NB. The differential equation for an ocean tracer y_k may be written in the general form:

$$V_k \frac{\mathrm{d}y_k}{\mathrm{d}t} = F_{\mathrm{thm}} + F_{\mathrm{gas}} + F_{\mathrm{bio}} + F_{\mathrm{in}} + F_{\mathrm{sed}} \ , \tag{2}$$

where V_k is the volume of box k and F's are fluxes due to (thermohaline) circulation and mixing, air-sea gas exchange (e.g. in case of TCO_2), biological uptake and remineralization, riverine/weathering input, and sediment fluxes. The first three flux terms on the right-hand side of Eq. (2) will be explained in the following subsections; the riverine/weathering and sediment flux terms will be explained in Sects. 4 and 6.

3.2.1 Circulation, mixing, and air-sea gas exchange

Given a prescribed ocean circulation- and mixing scheme, F_{thm} is of the form:

$$V_k \left(\frac{\mathrm{d}y_k}{\mathrm{d}t}\right)_{\mathrm{thm}} = T \sum_j (y_j - y_k) + \sum_l m_{lk}\ (y_l - y_k) \tag{3}$$

where T is the volume transport of the conveyor circulation and m_{lk} are mixing coefficients between boxes l and k (Fig. 2, Table 2). The box indices j and l are set by the prescribed circulation/mixing scheme (Fig. 2). The coefficients m_{lk} represent bidirectional mixing, hence $m_{lk} = m_{kl}$.

The air-sea gas exchange term reads:

$$V_k \left(\frac{\mathrm{d}y_k}{\mathrm{d}t}\right)_{\mathrm{gas}} = \kappa_{\mathrm{as}}\ A_k\ (p\mathrm{CO_2}^{\mathrm{a}} - P\mathrm{CO_2}^{k}) \tag{4}$$

where κ_{as} is the air-sea gas exchange coefficient for CO_2 and A_k is the area of surface box k; $p\mathrm{CO_2}^{\mathrm{a}}$ and $P\mathrm{CO_2}^{k}$ is the atmospheric pCO_2 and the pCO_2 in equilibrium with dissolved CO_2 in surface box k, respectively. The index k runs over all surface boxes for tracers such as TCO_2.

To derive the corresponding expression for the $^{13}CO_2$ flux, it is useful to rewrite κ_{as} as $\kappa_{\mathrm{as}} = u\ \beta$, where u is the gas transfer velocity and β the solubility (e.g. Siegenthaler and Münnich, 1981; Wanninkhof, 1985). Hence the air-sea CO_2 flux per unit area may be written as:

$$F_{\mathrm{gas}} = u\ (\beta \cdot p\mathrm{CO_2}^{\mathrm{a}} - [\mathrm{CO_2}]) \ , \tag{5}$$

where $[CO_2]$ is the concentration of dissolved CO_2 in solution. A similar equation holds for ^{13}C:

$$^{13}F_{\mathrm{gas}} = {}^{13}u\ ({}^{13}\beta \cdot p{}^{13}\mathrm{CO_2}^{\mathrm{a}} - [{}^{13}\mathrm{CO_2}]) \ . \tag{6}$$

Using $\alpha_u = {}^{13}u/u$ and $\alpha_{\mathrm{dg}} = {}^{13}\beta/\beta$, where α_u represents the kinetic fractionation during gas exchange and α_{dg} the equilibrium fractionation between dissolved and gaseous CO_2 (Mook, 1986; Zhang et al., 1995), it follows:

$$^{13}F_{\mathrm{gas}} = \kappa_{\mathrm{as}}\ \alpha_u\ (\alpha_{\mathrm{dg}} \cdot p{}^{13}\mathrm{CO_2}^{\mathrm{a}} - R_{\mathrm{d}}\ \beta^{-1}\ [\mathrm{CO_2}]) \ , \tag{7}$$

where $\kappa_{\mathrm{as}} = u\ \beta$ (see above) and R_{d} is the $^{12}C/^{13}C$ ratio of dissolved CO_2. R_{d} may be calculated taking into account the speciation and isotope fractionation among the various carbonate species (e.g. Wanninkhof, 1985; Zeebe and Wolf-Gladrow, 2001). Alternatively, a simplified expression for R_{d} may be obtained assuming that the carbon isotope ratio of HCO_3^- (R_{b}) is approximately equal to that of TCO_2 ($R_{\mathrm{b}} \simeq R_{\mathrm{T}}$). In other words, $R_{\mathrm{d}} \simeq \alpha_{\mathrm{db}}\ R_{\mathrm{T}}$, where α_{db} is the fractionation between dissolved CO_2 and HCO_3^- (Mook, 1986; Zhang et al., 1995). Over the pH range from 7.5 to 8.2 and at 20 °C, this approximation differs from the full calculation by 0.2 to

Table 2. Physical and biogeochemical parameters (ocean model).

Parameter	Symbol	Modern	P/E-setup[a]	Unit
Conveyor Transport	T	20[b]	25	Sv[c]
Tethys Transport	T_T	–	2	Sv
Upwelling (D–M)[d]	t_A, t_I	0.2,0.2[e,f]		–
Mixing (L–M)[d]	m_{lk}	21,17,25[g,f]	13,13,27[g,f]	Sv
Mixing (H–D)[d]	m_{lk}	4,3,10[g,f]	5,5,8[g,f]	Sv
Mixing Tethys	m_{lk}	–	12,1,8[h,f]	Sv
Temperature (initial)	T_C^0	20,10,2,2[i]	25,16,12,12[i]	°C
Temp. relax. time	τ_n	20,200,1000[j]		yr
Salinity	S	34.7		–
Gas exch. coeff. CO_2	κ_{as}	0.06[k]		$mol\,(\mu atm\,m^2\,yr)^{-1}$
Biopump-efficiency	f_{epl}	0.80[f]		–
Remin. fraction (M)[d]	f_{rim}	0.78[f]		–
Remin. fraction (D) [d]	$1 - f_{rim}$	0.22		–
P/C in C_{org}	REDPC	1/130		–
N/C in C_{org}	REDNC	15/130		–
O_2/C (C_{org}-remin.)	REDO2C	165/130		–
C-export (H)[d]	F_{eph}	1.8[f]		$mol\,m^{-2}\,yr^{-1}$
P-export (H)[d]	F_{pph}	$F_{eph} \times$ REDPC		$mol\,m^{-2}\,yr^{-1}$
Rain ratio[l]	r_{rain}	6.1	6.7[f]	–
$CaCO_3$ water dissol.[m]	ν_{wc}	0.31[f]		–

[a] Same as modern version unless indicated. [b] Toggweiler (1999). [c] $1\,Sv = 10^6\,m^3\,s^{-1}$. [d] L = Low-latitude surface, H = High-latitude surface, M = InterMediate, D=Deep. [e] Fraction upwelled into intermediate Atlantic, Indian (see Fig. 2). [f] Tuned. [g] Atlantic, Indian, Pacific. [h] (L−M Tethys, L−D Tethys, I-Tethys−I-Indian). [i] L, M, D, H-box. [j] Surface, intermediate, deep. [k] Broecker and Peng (1998). [l] C_{org} : $CaCO_3$. [m] Fraction of total $CaCO_3$ export dissolved in water column.

0.3 ‰. The simplified expression will thus suffice for most LOSCAR applications. Noting that $\beta^{-1} \cdot [CO_2] = PCO_2$, the air-sea gas-exchange term for $^{13}CO_2$ can then be written as:

$$V_k \left(\frac{dy_k}{dt} \right)_{gas} = \kappa_{as}\, A_k\, \alpha_u\, (\alpha_{dg}{}^k \cdot p^{13}CO_2{}^a - \alpha_{db}{}^k\, R_T^k \cdot PCO_2{}^k)\,. \quad (8)$$

This expression is readily evaluated in LOSCAR, which carries $p^{13}CO_2{}^a$, PCO_2, and $T^{13}CO_2$ as tracers (note that $R_T^k = T^{13}CO_2{}^k / TCO_2{}^k$). Values for the fractionation factors (α's) as functions of temperature have been summarized in the literature (Mook, 1986; Zhang et al., 1995; Zeebe and Wolf-Gladrow, 2001). The user can choose between the sets of fractionation factors given by Mook (1986) and Zhang et al. (1995). However, the differences between the two sets are minor, except for the fractionation between CO_3^{2-} and HCO_3^-, which is not used in LOSCAR given the simplified expressions above.

3.2.2 Biological pump

The biological uptake and recycling of tracers is parameterized based on phosphate (PO_4 for short). For instance, net uptake of PO_4 in the low-latitude surface ocean (equivalent to particle export flux from the mixed layer) is calculated as:

$$V_k \left(\frac{d[PO_4]_k}{dt} \right)_{upt} = F_{ppl}^k = -\, f_{epl}\, m_{jk}\, [PO_4]_j\,, \quad (9)$$

where the parameter f_{epl} describes the efficiency for PO_4 uptake in the low-latitude surface boxes, $m_{jk} \times [PO_4]_j$ is the flux of PO_4 supplied by upwelling/mixing from the underlying intermediate box j into the surface box k. (Note that in the model, the conveyor transport T does not directly supply nutrients to the warm surface waters; it does so, however, to the cold surface waters, see Fig. 2). If f_{epl} were to approach 1.0 (100 % efficiency), all upwelled PO_4 would be converted to sinking particles and the phosphate concentration of surface box k would be zero. In the model, as well as in reality, f_{epl} is usually less than 1.0 (Table 2). The fraction f_{rim} of the export flux is remineralized in the intermediate box, whereas the fraction $(1 - f_{rim})$ is remineralized in the deep box.

The high-latitude PO_4 export flux can be set directly by assigning a value to the flux parameter F_{pph}. If the value chosen is too large to be supported by the total PO_4 influx entering the H-box, simple Michaelis-Menten kinetics prevent PO_4 from becoming negative. Caution is therefore advised when increasing F_{pph} because the actual high-latitude export flux may be less than the value assigned to F_{pph}. The high-latitude export flux is remineralized in the deep boxes.

The fluxes of TCO_2 and TA due to biological uptake and recycling are computed based on PO_4 using a given Redfield-

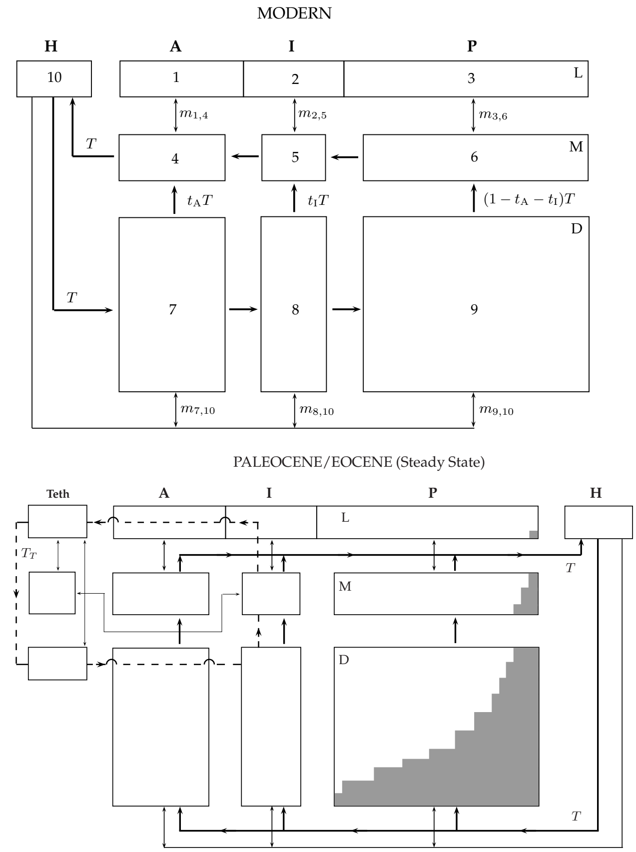

Fig. 2. Ocean circulation and mixing schemes implemented in LOSCAR for modern setup (top) and Paleocene/Eocene (P/E) steady-state (bottom). A = Atlantic, I = Indian, P = Pacific ocean, H = High-latitude surface, Teth = Tethys. L = Low-latitude surface, M = interMediate, D = Deep box. T represents the conveyor transport, while the coefficients m_{lk} represent bidirectional mixing between boxes. The generic H-box represents cold surface waters without reference to a specific location. Nevertheless, the modern setup is motivated by preindustrial circulation patterns with significant deep water formation in the North Atlantic (e.g. Walker and Kasting, 1992; Toggweiler, 1999). The P/E steady-state setup is inspired by observations and modeling studies of Paleocene/Eocene circulation patterns with significant deep water formation in the Southern Ocean (e.g. Bice and Marotzke, 2002; Thomas et al., 2003; Lunt et al., 2010). T_T (dashed line) represents the Tethys circulation, which connects to the Indian Ocean (note that the T_T-surface and deep branch do not flow through Atlantic boxes, as indicated by arcs). Note also that a transient contribution of North Pacific Deep Water (not shown) was included in our PETM simulations (Zeebe et al., 2009). All ocean boxes (except H-box) in the modern and P/E-setup are coupled to sediment boxes (schematically indicated only in the bottom panel for the Pacific by the gray shaded area).

and rain ratio (Table 2). Note that there is a small contribution to alkalinity changes from organic carbon production and respiration as a result of nitrate uptake and release (e.g. Zeebe and Wolf-Gladrow, 2001). The major contribution to alkalinity changes in the model is associated with $CaCO_3$ fluxes. Of the total $CaCO_3$ export flux, the larger fraction is destined for accumulation or dissolution in sediments, the latter of which returns total carbon and alkalinity to the ocean (Sect. 6). A smaller fraction of the $CaCO_3$ export is assumed to dissolve in the water column (Table 2). This assumption yields better agreement with observed TA fields and is consistent with observations and modeling studies indicating substantial water column dissolution above the lysocline (e.g. Archer et al., 1998; Milliman et al., 1999; Feely et al., 2002). In the model, the fraction representing $CaCO_3$ water column dissolution is added to the corresponding deep boxes, hence increasing TCO_2 and TA in these boxes.

The export flux of $T^{13}CO_2$ is determined based on the total carbon export flux and a carbon isotope fractionation factor representing the isotope effect associated with the fixation of organic matter. For example, in the low-latitude surface, the $T^{13}CO_2$ flux is computed as:

$$^{13}F^k_{\mathrm{epl}} = \alpha_{(\mathrm{Corg}-T)}\ R^k_{\mathrm{T}}\ F^k_{\mathrm{epl}} \tag{10}$$

where F^k_{epl} is the total carbon export flux from box k, $R^k_{\mathrm{T}} = \mathrm{T^{13}CO_2}^k/\mathrm{TCO_2}^k$, and $\alpha_{(\mathrm{Corg}-T)} = 0.9723$ represents the carbon isotope fractionation between organic carbon and TCO_2. The fractionation factor $\alpha_{(\mathrm{Corg}-T)}$, or more precisely its corresponding ε-value [$\varepsilon = (\alpha - 1)10^3$], should not be confused with the isotopic difference between the carbon source and fixed carbon, often denoted as ε_{p} (e.g. Hayes, 1993). While ε_{p} requires knowledge about the photosynthetic carbon source (e.g. CO_2 or HCO_3^-), $\varepsilon_{(\mathrm{Corg}-T)}$ does not. $\varepsilon_{(\mathrm{Corg}-T)}$ is a model-specific, tunable parameter representing a globally averaged value for the marine carbon isotope fractionation between organic carbon and TCO_2. It is tuned so as to reproduce the observed $\delta^{13}C$ distribution in the ocean. For the sake of simplicity, no fractionation is associated with the precipitation and dissolution of $CaCO_3$ in the model.

4 Carbonate and silicate weathering

Weathering of carbonate rocks on the continents takes up atmospheric CO_2 and supplies calcium and bicarbonate ions to the ocean:

$$\mathrm{CaCO_3 + H_2O + CO_2 \rightleftharpoons Ca^{2+} + 2\ HCO_3^-}\ . \tag{11}$$

Hence two moles of carbon and one mole of Ca^{2+} enter the ocean for each mole of $CaCO_3$ weathered, raising ocean TCO_2 and TA by two units each (Fig. 3). If the $CaCO_3$ riverine/weathering influx is denoted by F_{cc} (in units of mol $CaCO_3$ yr^{-1}, see Table 3), then:

$$V_k \left(\frac{\mathrm{d[TCO_2]}_k}{\mathrm{d}t}\right)_{\mathrm{cc}} = V_k \left(\frac{\mathrm{d[TA]}_k}{\mathrm{d}t}\right)_{\mathrm{cc}} = 2\ F_{\mathrm{cc}}\ \mathrm{NOC}^{-1} \tag{12}$$

where $k = 1, \ldots,$ NOC runs over all low-latitude surface boxes and NOC is the number of corresponding ocean basins. Note

Table 3. Weathering and sediment model parameters.

Parameter	Symbol	Value[a]	Unit
$CaCO_3$ weath. flux (initial)	F_{cc}^0	12[b] (16)	10^{12} mol yr^{-1}
$CaSiO_3$ weath. flux (initial)	F_{si}^0	5[c] (6)	10^{12} mol yr^{-1}
CO_2 degass. flux (initial)	F_{vc}^0	F_{si}^0	10^{12} mol yr^{-1}
$CaCO_3$ weath. exponent	n_{cc}	0.4[d]	–
$CaSiO_3$ weath. exponent	n_{si}	0.2[d]	–
δ^{13}C weath.	$\delta^{13}C_{in}$	1.5 (2.0)	‰
δ^{13}C degass.	$\delta^{13}C_{vc}$	-4	‰
Height sediment mixed layer	h_s	0.08	m
Density, solids	ρ_s	2.5×10^3	kg m^{-3}
non-$CaCO_3$ flux[e]	F_{rrf}	0.35×10^{-2}	kg m^{-2} yr^{-1}
Porosity, pure clay	ϕ_0	0.85[f]	–
Porosity, pure $CaCO_3$	ϕ_1	0.62[f]	–
Dissolution rate const. (eff.)[g]	K_{sd}	20.36×10^{10}	mol m^{-2} yr^{-1}
Dissolution rate order (eff.)[g]	n_{sd}	2.40	–

[a] Default: modern version, parentheses: P/E-version. [b] Morse and Mackenzie (1990). [c] Walker and Kasting (1992). [d] Uchikawa and Zeebe (2008). [e] Rain of refractory, non-$CaCO_3$ material to sediments. [f] See Zeebe and Zachos (2007). [g] Effective rate parameters, relating bottom water undersaturation to dissolution rate (Keir, 1982; Sundquist, 1986; Sigman et al., 1998; Zeebe and Zachos, 2007); n_{sd} is not to be confused with the calcite reaction order n, relating porewater undersaturation to dissolution rate (typically $n = 4.5$).

that in steady state, subsequent precipitation of $CaCO_3$ in the ocean (Reaction 11 backwards) releases the same amount of CO_2 back into the atmosphere as was taken up during weathering. In other words, the CO_2 for carbonate weathering essentially originates from the ocean (Fig. 3). As a result, although the addition of Ca^{2+} and 2 HCO_3^- increases ocean TCO_2 : TA in a 2:2 ratio, on a net basis $CaCO_3$ weathering increases ocean TCO_2 : TA in a 1:2 ratio because one mole of CO_2 returns to the atmosphere. If influx equals burial, carbonate weathering thus represents a zero net balance for atmospheric CO_2. The steady-state balance is restored after a perturbation on a time scale of 5 to 10 kyr and is referred to as “calcite compensation” (Broecker and Peng, 1987; Zeebe and Westbroek, 2003).

Weathering of silicate rocks and simultaneous uptake of atmospheric CO_2 may be described by:

$$CaSiO_3 + H_2O + 2\ CO_2 \rightleftharpoons Ca^{2+} + 2HCO_3^- + SiO_2\ . \quad (13)$$

If the $CaSiO_3$ riverine/weathering influx is denoted by F_{si} (in units of mol $CaSiO_3$ yr^{-1}, see Table 3), then:

$$V_k \left(\frac{d[TCO_2]_k}{dt}\right)_{si} = V_k \left(\frac{d[TA]_k}{dt}\right)_{si} = 2\ F_{si}\ NOC^{-1}\ . \quad (14)$$

Note that silicate weathering removes 2 moles of CO_2 from the atmosphere for each mole of $CaSiO_3$ weathered. Subsequent precipitation and burial of $CaCO_3$ (Reaction 11 backwards) releases one mole of CO_2 back to the atmosphere, the other mole is buried in the form of $CaCO_3$ in sediments (Fig. 3). In steady state, the balance is closed by long-term CO_2 input to the atmosphere from volcanic degassing. Putting it the other way, the CO_2 released by volcanoes is balanced by silicate weathering and subsequent carbonate burial in the ocean (Fig. 3). The net reaction is:

$$CaSiO_3 + CO_2 \rightleftharpoons CaCO_3 + SiO_2\ . \quad (15)$$

The steady-state balance for silicate weathering is restored after a perturbation on a time scale of 10^5 to 10^6 yr. This process also restores the partial pressure of atmospheric CO_2 in order to maintain a mass balance of long-term carbon cycle fluxes (e.g. Berner et al., 1983; Zeebe and Caldeira, 2008).

The restoring time scale for silicate weathering is much longer than for carbonate weathering for two reasons. First, silicate weathering requires whole-ocean TCO_2 to adjust, whereas carbonate weathering only requires the ocean’s carbonate ion concentration to adjust (e.g. Zeebe and Westbroek, 2003). On average, the modern TCO_2 inventory is about 20 times larger than mean-ocean $[CO_3^{2-}]$ (e.g. Broecker and Peng, 1998). Second, carbonate weathering fluxes have been estimated to be about 2.5-times larger than silicate weathering fluxes (Table 3; Morse and Mackenzie, 1990; Walker and Kasting, 1992). Combined, this gives a factor of about 50, which, multiplied by the calcite compensation time scale of 10 kyr, gives 500 kyr, which is about right.

4.1 Weathering feedback

The feedback between atmospheric CO_2 and weathering fluxes of carbonates and silicates is parameterized in the model using the following equations (see Walker et al., 1981; Berner et al., 1983; Walker and Kasting, 1992):

$$F_{cc} = F_{cc}^0 \left(pCO_2/pCO_2^0\right)^{n_{cc}} \quad (16)$$

$$F_{si} = F_{si}^0 \left(pCO_2/pCO_2^0\right)^{n_{si}} \quad (17)$$

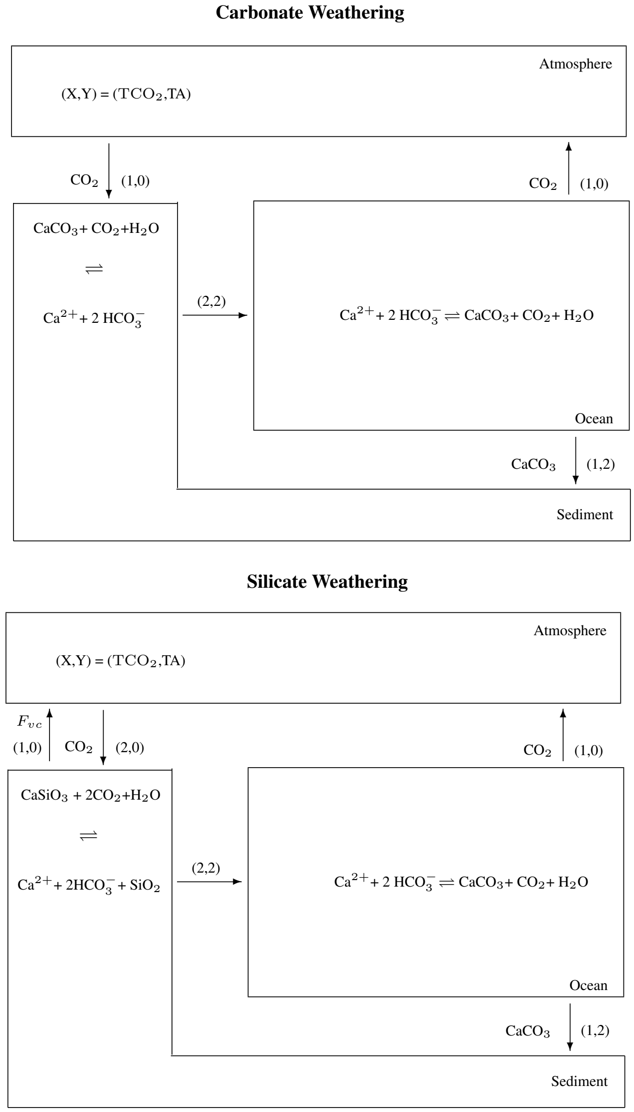

Fig. 3. Schematic illustration of carbonate and silicate weathering fluxes. Numbers in parentheses indicate steady-state fluxes of TCO_2 and TA in mole per mole of $CaCO_3$ or $CaSiO_3$ weathered.

where the superscript "0" refers to the initial (steady-state) value of the weathering flux and pCO_2, respectively. The parameters n_{cc} and n_{si} control the strength of the weathering feedback (Table 3). The default values for n_{cc} and n_{si} adopted in LOSCAR were chosen so as to represent conservative values, resulting in a weak default weathering feedback at the lower end of the spectrum (see Fig. 1 in Uchikawa and Zeebe, 2008). The user is welcome to change and vary these parameters values (cf. Uchikawa and Zeebe, 2008; Komar and Zeebe, 2011).

As mentioned above, in steady state, the silicate weathering flux balances the CO_2 degassing flux from volcanism:

$$F_{si}^0 = F_{vc}^0 \, . \quad (18)$$

Thus, the long-term steady-state pCO_2 of the model is set by picking a value for pCO_2^0, which drives the system towards equilibrium via the silicate weathering equation (Eq. 17). Only when the actual model pCO_2 equals pCO_2^0, will the fluxes be balanced ($F_{si} = F_{si}^0 = F_{vc}^0$). The carbon isotope composition of the volcanic degassing flux is set to −4.0 ‰ in the model, while the $\delta^{13}C$ of the weathering flux is set to 1.5 ‰ and 2.0 ‰ for the modern and P/E-setup, respectively (see Table 3).

5 Atmosphere

The model variable tracking the inventory of atmospheric carbon dioxide, C_{atm}, is related to the partial pressure of CO_2 in the atmosphere by (analogous for ^{13}C):

$$C_{atm} = pCO_2{}^{a} \times q^0 \quad (19)$$
$$^{13}C_{atm} = p^{13}CO_2{}^{a} \times q^0 \quad (20)$$

where $q^0 = (2.2\times10^{15}/12)$ mol µatm^{-1} converts from µatm to mol. Note that for numerical scaling purposes (see Sect. 7.4), C_{atm} is normalized to order 1 in the program by multiplying by $(A_{oc} \times 100)^{-1}$ (arbitrary factor). The differential equations for C_{atm} and $^{13}C_{atm}$ may be written in the general form:

$$\frac{d\, C_{atm}}{dt} = F_{gas} + F_{vc} - F_{cc} - 2\, F_{si} + C'_{in} \quad (21)$$
$$\frac{d\, ^{13}C_{atm}}{dt} = {}^{13}F_{gas} + {}^{13}F_{vc} - {}^{13}F_{cc} - 2\, {}^{13}F_{si} + {}^{13}C'_{in} \, , \quad (22)$$

where F's are fluxes due to air-sea gas exchange, volcanic input and weathering (see Sect. 4), and possible carbon input sources. Fluxes of ^{13}C due to volcanic degassing and weathering are calculated from $^{13}F_j = R_j\ F_j$, where $R_j = R_{std}(\delta^{13}C_j/1\times10^3 + 1)$ and $\delta^{13}C_j$ is set to −4.0 ‰ and 1.5 ‰, respectively, for the modern version (see Table 3).

The air-sea gas exchange terms for the atmosphere read:

$$\left(\frac{d\, C_{atm}}{dt}\right)_{gas} = \sum_k \kappa_{as}\, A_k\, (PCO_2{}^{k} - pCO_2{}^{a}) \quad (23)$$

$$\left(\frac{d\, ^{13}C_{atm}}{dt}\right)_{gas} = \sum_k \kappa_{as}\, A_k\, \alpha_u (\alpha_{db}{}^{k}\, R_T^k \cdot PCO_2{}^{k} - \alpha_{dg}{}^{k} \cdot p^{13}CO_2{}^{a}) \quad (24)$$

where κ_{as} is the air-sea gas exchange coefficient for CO_2 and A_k is the area of surface box k; $pCO_2{}^{a}$ and $PCO_2{}^{k}$ is the atmospheric pCO_2 and the pCO_2 in equilibrium with dissolved CO_2 in surface box k, respectively. For details regarding the gas-exchange term for ^{13}C, see Sect. 3.2.1. The sum runs over all surface boxes. In case of carbon input to

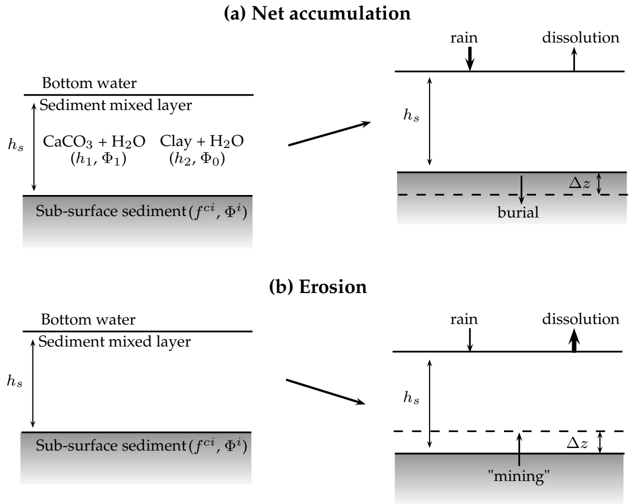

Fig. 4. Schematic representation of the sediment model. The sediment mixed layer (thickness h_s) can be separated into pure calcite plus pore water (thickness h_1, porosity ϕ_1) and pure clay plus pore water (thickness h_2, porosity ϕ_0). **(a)** Net accumulation equals $CaCO_3$ rain minus dissolution. At the bottom of the sediment mixed layer, an amount equal to net accumulation is removed via burial (Δz). **(b)** If dissolution of $CaCO_3$ exceeds the rain of $CaCO_3$ plus clay, chemical erosion occurs. Previously deposited, underlying sediment is reintroduced into the top layer and exposed to dissolution ("mining"). Sub-surface sediment properties are based on the initial steady-state configuration (f^{ci} and ϕ^i is the initial calcite fraction and porosity, respectively).

the atmosphere from fossil fuel burning or from other carbon sources, for instance, during the PETM, terms of the form:

$$\left(\frac{\mathrm{d}\,C_{\mathrm{atm}}}{\mathrm{d}t}\right)_{C_{\mathrm{in}}} = C_{\mathrm{in}} \times 10^{15}/12 \qquad (25)$$

$$\left(\frac{\mathrm{d}\,{}^{13}C_{\mathrm{atm}}}{\mathrm{d}t}\right)_{C_{\mathrm{in}}} = {}^{13}C_{\mathrm{in}} \times 10^{15}/12 \qquad (26)$$

are added where C_{in} is in units of Pg C yr^{-1} and ${}^{13}C_{\mathrm{in}} = R_{\mathrm{in}}\,C_{\mathrm{in}}$, where R_{in} is the carbon isotope ratio of the carbon source.

6 Sediments

The sediment model calculates $\%CaCO_3$ (dry weight) in the seafloor-bioturbated (mixed) sediment layer of thickness h_s as a function of sediment rain, dissolution, burial, and chemical erosion (for more details see Fig. 4 and Zeebe and Zachos, 2007). The model is particularly useful for long-term integrations and has been constructed similar to other models of this class (e.g. Keir, 1982; Sundquist, 1986; Sigman et al., 1998). However, the current model also includes variable porosity – a feature critical to simulating strong dissolution events that lead to sediment erosion, such as expected for the future or during the PETM (Zeebe and Zachos, 2007; Zeebe et al., 2008, 2009).

6.1 Chemical erosion

When dissolution of $CaCO_3$ exceeds the rain of $CaCO_3$ plus refractory material such as clay, the sediment column shrinks and previously deposited, underlying sediment is reintroduced into the top layer and exposed to dissolution. This is referred to as chemical erosion (Fig. 4). As a result, significantly more $CaCO_3$ is available for dissolution during erosion than originally contained in the top sediment layer. Once the top layer is entirely filled with clay, the sediment column is "sealed" and dissolution ceases. In order to fill the sediment top layer with clay, the sediment volume that was initially filled with $CaCO_3$ + pore water must be replaced by clay + pore water. Thus, if the sediment porosity ϕ is constant, the ratio of total $CaCO_3$ available during erosion to the mass contained in the original surface layer is given by:

$$1 + \frac{f^{ci}}{(1 - f^{ci})} \qquad (27)$$

(Broecker and Takahashi, 1977) where f^{ci} and $(1 - f^{ci})$ are the initial $CaCO_3$ and clay dry weight fraction of the sediment, respectively. However, if porosity varies with $\%CaCO_3$ (as observations show, see below), the ratio of total dissolved to initial $CaCO_3$ is given by:

$$1 + \frac{1-\phi_0}{1-\phi_1}\,\frac{f^{ci}}{1-f^{ci}} \qquad (28)$$

where ϕ_0 and ϕ_1 are the porosities of a pure clay and calcite layer, respectively. The factor $(1-\phi_0)/(1-\phi_1)$ is of the order 0.3–0.5 and therefore significant as it reduces the erodible $CaCO_3$ from below the bioturbated layer by 50–70 % compared to the constant ϕ estimate (Archer, 1996). In LOSCAR, chemical erosion is included based on Eq. (37), see below.

6.2 Variable porosity

In many locations, it has been observed that porosity decreases with greater $CaCO_3$ fraction f^c (e.g. Mayer, 1991; Herbert and Mayer, 1991; deMenocal et al., 1993). That is, sediment with high $CaCO_3$ content has a higher concentration of total solids per unit volume than low carbonate sediment. The relationship between ϕ and f^c for a sediment layer composed of $CaCO_3$, clay, and pore water is given by:

$$\phi = \frac{\phi_0 + f^c\,F_\phi}{1 + f^c\,F_\phi} \qquad (29)$$

where $F_\phi = (\phi_1 - \phi_0)/(1-\phi_1)$. The sediment model uses variable porosity as given by Eq. (29) and values for ϕ_0 and ϕ_1 as given in Table 3. Note that using the non-linear Eq. (29) in the model leads to the correct ratio of initial to erodible

$CaCO_3$ (cf. Eq. 28, which was independently derived based on the geometry of the problem), while a linear relationship, for instance, would not.

6.3 Sediment model equations (single sediment box)

At every time step, calcite and clay rain of solid density ρ_s is added to the top sediment layer of thickness h_s (see Table 3 for values). Dissolution of calcite reduces the calcite content and net accumulation is hence rain minus dissolution (Fig. 4). At the bottom of the sediment mixed layer, an amount equal to net accumulation is removed via burial. If dissolution of $CaCO_3$ exceeds the rain of $CaCO_3$ plus clay, chemical erosion occurs. The sediment model thus has to provide equations to calculate rain, dissolution, burial, and erosion. At variable porosity, the top layer can be separated into pure calcite plus pore water at porosity ϕ_1 (volume $= Ah_1$) and pure clay plus pore water at porosity ϕ_0 (volume $= Ah_2$). For variable porosity, the model equations can be conveniently written in terms of $\mathrm{d}h_1/\mathrm{d}t$. Conversion to $\mathrm{d}f^c/\mathrm{d}t$ merely requires multiplication by a factor (see below).

In case rain exceeds dissolution, no erosion needs to be considered and we can write for a single sediment box:

$$\frac{\mathrm{d}h_1}{\mathrm{d}t} = r^{cs} - r^{d} - w^{c} \tag{30}$$

where r^{cs} is the calcite rain rate, r^d is the calcite dissolution rate, and w^c is the calcite burial rate. All rates refer to volume of calcite plus pore water per unit area and time (unit $\mathrm{m\,yr^{-1}}$) at porosity ϕ_1. Total rates of calcite + clay + pore water are denoted by r^s and w. Burial equals rain minus dissolution, i.e. $w = r^s - r^d$, and the condition for no erosion is $w > 0$. The rain rate of calcite, r^{cs}, depends on the carbon export, the rain ratio, and the fraction of water column dissolution. In the low latitudes, for instance, r^{cs} is given by:

$$r^{cs} = F_{epl}\, {r_{rain}}^{-1}\, (1-\nu_{wc}) \times k^* \tag{31}$$

where F_{epl} is the low-latitude carbon export (in units of $\mathrm{mol\,m^{-2}\,yr^{-1}}$), r_{rain} is the rain ratio (C_{org} : $CaCO_3$), ν_{wc} is the $CaCO_3$ fraction dissolved in the water column (Table 2), $k^* = k^0/[\rho_s\,(1-\phi_1)]$ converts from $\mathrm{mol\,m^{-2}\,yr^{-1}}$ to $\mathrm{m\,yr^{-1}}$, and $k^0 = (100/10^3)\,\mathrm{kg\,mol^{-1}}$ converts from mol $CaCO_3$ to kg $CaCO_3$. The rain rate of refractory material, r^{rs}, is calculated correspondingly based on F_{rrf} (Table 3) and the total rain r^s is given by $r^s = r^{cs} + r^{rs}$.

The dissolution rate, r^d, is calculated as:

$$r^{d} = \mathcal{R}^{d} \times k^* , \tag{32}$$

where $\mathcal{R}^d$ is given by the following expression at modern seawater Mg/Ca ratio (Keir, 1982; Sigman et al., 1998):

$$\mathcal{R}^{d} = (f^c)^{0.5}\, K_{sd}\, ([CO_3^{2-}]_{sat} - [CO_3^{2-}])^{n_{sd}}\, (c^0)^{-n_{sd}}$$
$$\text{if } [CO_3^{2-}] < [CO_3^{2-}]_{sat} \tag{33}$$

$$\mathcal{R}^{d} = 0 \quad \text{otherwise} , \tag{34}$$

where K_{sd} and n_{sd} are "effective" rate parameters (see below), $[CO_3^{2-}]_{sat}$ and $[CO_3^{2-}]$ is the carbonate ion concentration at calcite saturation and in the bottom water, respectively, and $c^0 = 1\,\mathrm{mol\,kg^{-1}}$ so that $\mathcal{R}^d$ is in units of $\mathrm{mol\,m^{-2}\,yr^{-1}}$. It is important to note that the effective rate parameters K_{sd} and n_{sd} relate *bottom* water undersaturation to dissolution rate (Keir, 1982; Sundquist, 1986; Sigman et al., 1998; Zeebe and Zachos, 2007, see Table 3 for values). They are not to be confused with reaction parameters relating *porewater* undersaturation to dissolution rate such as the calcite reaction order n (typically $n = 4.5$).

Finally, an expression is needed for the calcite burial, w^c, as a function of total burial w. The thickness of the pure calcite layer within $\Delta z (= w\ \Delta t)$ can be expressed as $f^c\ \Delta z\ (1-\phi)$ but also as $1 \cdot \Delta h_1\ (1-\phi_1)$ (calcite fraction $=$ 1), which gives:

$$\Delta h_1 = f^c\ \Delta z\ \frac{1-\phi}{1-\phi_1} \tag{35}$$

or expressed per unit time as a rate:

$$w^c = f^c\ w\ \frac{1-\phi}{1-\phi_1} . \tag{36}$$

As a result, all rates have now been expressed by model-predicted quantities and thus by inserting Eqs. (31), (32), and (36) into (30), the change in calcite content per time step can be computed. Because we took care of all individual porosities, the relationship between ϕ and f^c, Eq. (29), is obeyed automatically.

In case of erosion ($w < 0$), it can be shown that:

$$\frac{\mathrm{d}h_1}{\mathrm{d}t} = -(1-f^{ci})\ (-w)\ \frac{1-\phi^i}{1-\phi_0} - r^{rs} \tag{37}$$

where f^{ci} and ϕ^i is the initial calcite fraction and porosity, respectively, and r^{rs} is the clay rain rate (see above). Subsurface sediment properties are hence based on the initial steady-state configuration (Fig. 4). For model applications that require multiple dissolution cycles with varying conditions during accumulation, the model should be restarted with appropriate initial conditions. The total dissolution of pure calcite can be derived as:

$$\frac{\mathrm{d}h^{dc}}{\mathrm{d}t} = [(-w) + r^s]\ (1-\phi_1) . \tag{38}$$

In other words, all calcite in Δz and calcite rain is dissolved. In addition, calcite is being replaced by the clay in Δz and by the clay rain (equivalent calcite is also dissolved).

Finally, the sediment model can also be formulated in terms of f^c by simply multiplying by a factor:

$$\frac{\mathrm{d}f^c}{\mathrm{d}t} = \frac{\mathrm{d}h_1}{\mathrm{d}t}\ G^{-1} = (r^{cs} - r^{d} - w^{c})\ G^{-1} , \tag{39}$$

where

$$G = \frac{h_s}{1-\phi_1} \left[(1-\phi) - f^c \frac{\partial \phi}{\partial f^c} \right] \tag{40}$$

and

$$\frac{\partial \phi}{\partial f^{\mathrm{c}}} = \frac{F_\phi\ (1-\phi_0)}{(1+f^{\mathrm{c}}\ F_\phi)^2} \tag{41}$$

with $F_\phi = (\phi_1 - \phi_0)/(1-\phi_1)$.

6.4 Sediment model equations (all sediment boxes)

Let y_n be a subset of $\boldsymbol{y}$ (Eq. 1), representing the $CaCO_3$ dry fraction (f^{c}) in sediment boxes at different depth levels in the different ocean basins. If the total number of depth levels is NSD and the total number of ocean basins is NOC (Table 1), then the total number of equations for all sediment boxes (total carbon) is NSD $\times$ NOC. Based on Eq. (39), the differential equation for the $CaCO_3$ dry fraction in sediment box j is (analogous equations hold for $Ca^{13}CO_3$):

$$\frac{\mathrm{d}y_n}{\mathrm{d}t} = \frac{\mathrm{d}(f^{\mathrm{c}}_j)}{\mathrm{d}t} = (r^{\mathrm{cs}}_j - r^{\mathrm{d}}_j - w^{\mathrm{c}}_j)\ G_j{}^{-1} \tag{42}$$

where $j = 1, 2, \ldots,$ NSD for the first ocean basin (Atlantic), $j =$ NSD $+1$, NSD $+2, \ldots, 2$ NSD for the second ocean basin (Indian), and so on. In case of dissolution, TCO_2 and TA are returned to the ocean, giving rise to the sediment source term in the ocean tracer equation (cf. Eq. 2):

$$V_k \left(\frac{\mathrm{d}[\mathrm{TCO_2}]_k}{\mathrm{d}t}\right)_{\mathrm{sed}} = \sum_j A^{\mathrm{sed}}_j\ \mathcal{R}^{\mathrm{d}}{}_j \tag{43}$$

$$V_k \left(\frac{\mathrm{d}[\mathrm{TA}]_k}{\mathrm{d}t}\right)_{\mathrm{sed}} = 2 \sum_j A^{\mathrm{sed}}_j\ \mathcal{R}^{\mathrm{d}}{}_j \tag{44}$$

where each sum runs over all sediment boxes j located within the area and depth range of ocean box k. The surface area of sediment box j is denoted by A^{sed}_j.

7 Miscellaneous

7.1 Ocean carbonate chemistry

Carbonate chemistry parameters for modern seawater composition are calculated based on equilibrium constants on the total pH scale (Lueker et al., 2000; Zeebe and Wolf-Gladrow, 2001). The C program uses a simplified and fast numerical routine to compute CO_2 parameters from TCO_2 and TA (Follows et al., 2006). If applied properly, the method yields accurate results that are essentially identical to those obtained with standard routines (Zeebe and Wolf-Gladrow, 2001). The method was originally devised to compute modern carbonate chemistry parameters in biogeochemical models where conditions change little between consecutive time steps (Follows et al., 2006). This is not necessarily always the case in LOSCAR and can lead to failure in rare cases. For instance, if the model is initiated with a very high TA/TCO_2 ratio, the calculated H^+ concentration may become negative. The user is warned in such instances and is advised to change the initial conditions. Again, such cases are probably rare. In fairness, it should also be noted that non-standard chemistry conditions (which can occur in LOSCAR), are beyond the original intend of the method (Follows et al., 2006). Apart from the limitation mentioned above, the method is easy to implement, sufficiently accurate, and computationally efficient.

7.2 Paleocene/Eocene ocean chemistry

Paleocene/Eocene seawater conditions were different from modern conditions owing to factors such as temperature and major ion composition of seawater, including the seawater Mg/Ca ratio (e.g. Tyrrell and Zeebe, 2004). These factors can significantly affect thermodynamic quantities such as equilibrium constants and solubility products, which in turn have a major impact on the predicted ocean carbonate chemistry and atmospheric CO_2. The chemistry routines implemented in LOSCAR allow for variations in, for instance, temperature, salinity, and the concentrations of Mg^{2+} and Ca^{2+} in seawater. For example, due to warmer surface and bottom water temperatures in the late Paleocene and Eocene, the calcite saturation concentration at a bottom water temperature of 14–17 °C during the PETM is quite different from the modern at 2 °C (see Fig. 3 of Zeebe and Zachos, 2007). This effect is included in LOSCAR by using temperature-dependent equations for the solubility product of carbonate minerals (Mucci, 1983). Pressure corrections for solubility products and equilibrium constants are based on Millero (1995) and references therein; for the latest revisions, check: www.soest.hawaii.edu/oceanography/faculty/zeebe_files/CO2_System_in_Seawater/csys.html.

Furthermore, the P/E-simulations use $[Mg^{2+}] = 30\,\mathrm{mmol\,kg^{-1}}$ and $[Ca^{2+}] = 20\,\mathrm{mmol\,kg^{-1}}$ rather than the modern values of $[Mg^{2+}] = 53\,\mathrm{mmol\,kg^{-1}}$ and $[Ca^{2+}] = 10\,\mathrm{mmol\,kg^{-1}}$ (Tyrrell and Zeebe, 2004; Zeebe et al., 2009). The effect of seawater Mg^{2+} and Ca^{2+} on the first and second dissociation constant of carbonic acid is estimated using sensitivity coefficients (Ben-Yaakov and Goldhaber, 1973):

$$s_{K^*} = \frac{\Delta K^*/K^*}{\Delta c_i/c_i} \tag{45}$$

where ΔK^* is the change in the dissociation constant K^* due to the relative change in concentration, $\Delta c_i/c_i$, of component i. Using $\Delta c/c = (c - c_{\mathrm{m}})/c_{\mathrm{m}}$, where m = modern, it follows:

$$\Delta K^* = s_{K^*}\ K^*\ (c/c_{\mathrm{m}} - 1) \tag{46}$$

and finally:

$$K^* = K^*_{\mathrm{m}} + \Delta K^*_{\mathrm{Mg^{2+}}} + \Delta K^*_{\mathrm{Ca^{2+}}}\ . \tag{47}$$

Sensitivity parameters for the effect of Mg^{2+} and Ca^{2+} on K^* are (Ben-Yaakov and Goldhaber, 1973):

$$s_{K_1^*} = 155 \times 10^{-3} \qquad s_{K_2^*} = 442 \times 10^{-3} \qquad \text{for } Mg^{2+} \quad (48)$$

$$s_{K_1^*} = 33.73 \times 10^{-3} \qquad s_{K_2^*} = 38.85 \times 10^{-3} \qquad \text{for } Ca^{2+}\,. \quad (49)$$

With these sensitivity parameters, and the modern and paleo-concentrations of Mg^{2+} and Ca^{2+} (see above), the correction to equilibrium constants (Eq. 47) can be applied.

Seawater Mg^{2+} and Ca^{2+} also affect the calcite solubility product, K^*_{sp}, and thus the steady-state deep-sea $[CO_3^{2-}]$. Following Mucci and Morse (1984), the stoichiometric solubility product drops with decreasing seawater Mg/Ca ratio. In other words, Eocene K^*_{sp} would have been smaller and, given roughly constant deep-sea saturation state, $[CO_3^{2-}]$ would also have been smaller than modern. The data of Mucci and Morse (1984) may be fitted to an equation of the form:

$$K^*_{sp} = K^*_{sp,m}\,[1 - \alpha\,(x_m - x)] \qquad (50)$$

where m = modern, $\alpha = 0.0833$, and x = Mg/Ca. Using modern and P/E-values for $[Mg^{2+}]$ and $[Ca^{2+}]$ as given above, the stoichiometric solubility product of calcite would have been reduced by about 30 %, compared to modern.

Another important consequence of changes in oceanic Ca^{2+}, for instance, is its effect on the ocean carbon inventory. The long-term carbon inventory and carbonate chemistry of the ocean-atmosphere system is controlled by atmospheric CO_2 and the balance between riverine flux and carbonate burial (Zeebe and Caldeira, 2008). Carbonate burial is tied to the deep-sea carbonate saturation, which is proportional to the product of $[Ca^{2+}] \times [CO_3^{2-}]$. If oceanic $[Ca^{2+}]$ doubles at constant saturation state, $[CO_3^{2-}]$ would drop by 50 % (even more if the effect of Mg/Ca on K^*_{sp} is accounted for). For example, $[CO_3^{2-}]$ prior to the PETM was hence much lower than modern if Paleocene/Eocene $[Ca^{2+}]$ was 20 mmol kg^{-1}. In the model, this leads to a pre-PETM ocean carbon inventory that is similar to the modern value, despite a higher baseline atmospheric CO_2 at the time.

7.3 Temperature sensitivity

The initial temperature of each individual ocean box is set at the start of the run. Throughout the run, temperature can be held constant, be manipulated based on user input, or be computed based on a simple expression for the sensitivity of temperature to changes in atmospheric CO_2 as calculated by the model (cf. Archer, 2005). In order to provide a flexible and numerically stable option, the C version of the program includes temperature as an ocean tracer variable. The temperature of ocean box k ($T_{C,k}$ in °C) is assumed to respond to a change in pCO_2 with a certain time lag and relax towards equilibrium temperature. The equilibrium temperature of box k is given by:

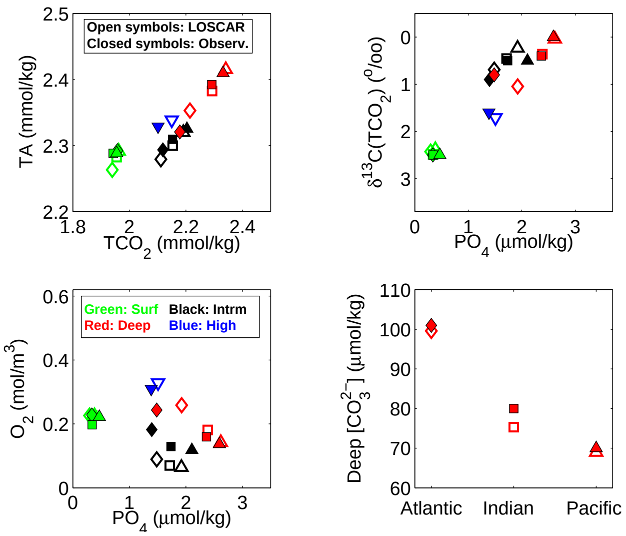

Fig. 5. Computed model tracers and observations used for LOSCAR parameter tuning for modern (preindustrial) configuration, see text for details.

$$T^{eq}_{C,k} = T^0_{C,k} + s\,\ln\left(pCO_2/pCO_2^0\right)/\ln(2)\,, \qquad (51)$$

where the superscript "0" refers to the initial (steady-state) temperature and pCO_2, respectively, and s is the prescribed temperature increase per doubling of atmospheric CO_2. The parameter s as used here is conceptually similar to what is generally referred to as "climate sensitivity". However, the precise meaning of s will have to be defined properly for each specific application in the context of the time scales and feedbacks involved (see Zeebe, 2011).

The differential equation for the temperature of ocean box k then reads:

$$\frac{d(T_{C,k})}{dt} = \left(T^{eq}_{C,k} - T_{C,k}\right)/\tau_n \qquad (52)$$

where τ_n is the relaxation time, which can take on three different values depending on whether k refers to a surface, intermediate, or deep box (Table 2).

7.4 Numerics

As mentioned above, the equations solved in LOSCAR are typically stiff and require an appropriate solver for the problem. The LOSCAR C-version uses a fourth-order Rosenbrock method with automatic stepsize adjustment (Press et al., 1992). For these kind of solvers, it is critical to scale the variables properly. Thus, variables have been scaled to order 1, if necessary, by multiplying by arbitrary factors before passing to the solver. This includes, for instance, atmospheric carbon and temperature (see Sects. 5 and 7.3).

The carbonate dissolution rate, $\mathcal{R}^d$ is proportional to the square root of the $CaCO_3$ fraction f^c (Eq. 33). It turned out

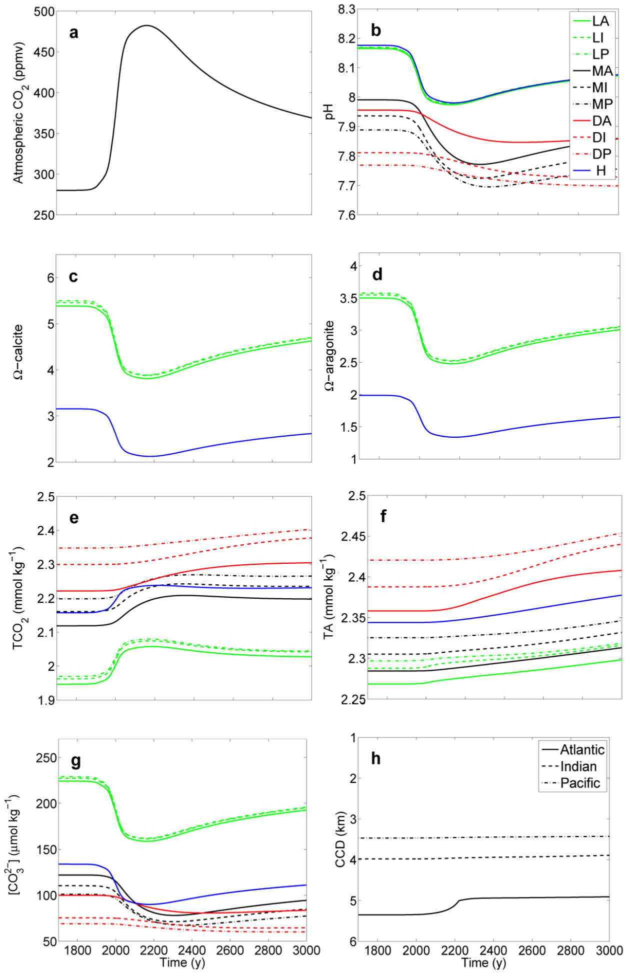

Fig. 6. Example of a fossil fuel emission scenario simulated in LOSCAR: total release of 1000 Pg C over 500 yr (see Zeebe et al., 2008). Results shown slightly differ from those in Zeebe et al. (2008) because ocean temperature was held constant here for simplicity. L = Low-latitude, M = interMediate, D = Deep, H = High-latitude. A = Atlantic, I = Indian, P = Pacific. Note that the step in the Atlantic calcite compensation depth (CCD, panel **h**) is due to the spacing of sediment-box depth levels in the model (adding more sediment boxes would make the curve smoother).

that during strong dissolution, f^c occasionally became negative when the $CaCO_3$ fraction approached zero. This issue has been eliminated (in most cases) by using a linear relationship between f^c and $\mathcal{R}^d$ when f^c drops below a certain threshold value f^c_{sml}. The threshold value can be changed by the user and should be increased if f^c still becomes negative during a run. Another option is to increase the solver accuracy by reducing the value of ε_{slv} (the default value is usually not very accurate).

LOSCAR is quick. Running the fossil fuel scenario over 1250 yr (Fig. 6) using the LOSCAR C code compiled under Linux with gcc 4.4.3, without optimization and default ε_{slv}, takes less than 2 s wall clock time on a current standard desktop machine with Intel Core2 Duo E8500 @3.16 GHz (no other CPU-demanding processes running). The computational efficiency makes LOSCAR an ideal tool for multi-parameter variations that require a large number of model runs (e.g. Zeebe et al., 2008, 2009).

8 Tuning

In order for LOSCAR to provide model output that resembles observations, several model parameters require tuning. This includes mixing coefficients, biological export fluxes, remineralization fraction (intermediate vs. deep box), rain ratio, and water column dissolution (see Table 2). The tuning is based on comparison between model-predicted variables and modern observations. For example, parameters were tuned by requiring the ocean tracer variables TCO_2 and TA in the various model boxes to match GLODAP data, averaged over the area and depth range of the corresponding boxes (Key et al., 2004). Note that TCO_2 data were corrected for anthropogenic carbon by subtracting 45 and 25 µmol kg^{-1} from the surface and intermediate values, respectively (see below for δ^{13}C-corrections). The agreement between model and data is satisfactory (see Fig. 5). As a result, the global preindustrial TCO_2 inventory in LOSCAR is 35 830 Pg C vs. 35 760 Pg C based on GLODAP data (Key et al., 2004). Similarly, model PO_4 and oxygen were compared to data summarized in the World Ocean Atlas (WOA05, 2005). Again, the agreement between model and data is adequate, except perhaps for the oxygen content in intermediate boxes, which appears to be underestimated by the model. This could be improved. However, it would come at the expense of a larger mismatch in the deep boxes. This was avoided because for our LOSCAR applications so far, the properties of the deep boxes were more important than those of the intermediate boxes.

Another variable used for parameter tuning is the stable carbon isotope composition of TCO_2 ($\delta^{13}C_{TCO_2}$), which was matched to the data of Kroopnick (1985). Note that due to the ocean's uptake of fossil fuel carbon (which is isotopically light, i.e. depleted in ^{13}C), the ocean's $\delta^{13}C_{TCO_2}$ is continuously dropping (so-called Suess effect). Thus, for preindustrial tuning, the early δ^{13}C-data sets are more useful than the most recent ones, which are increasingly contaminated with anthropogenic carbon. Nevertheless, Kroopnick (1985) estimated that surface ocean $\delta^{13}C_{TCO_2}$ had already dropped by ∼0.5 ‰ and that the average $\delta^{13}C_{TCO_2}$ of the preindustrial surface ocean was about 2.5 ‰. This surface value was used for model parameter tuning (Fig. 5). As a result, the preindustrial δ^{13}C of atmospheric CO_2 is −6.38 ‰ in LOSCAR vs. −6.30 to −6.40 ‰ based on ice core and firn data (e.g. Francey et al., 1999).

Adequate model values for the steady-state carbonate ion concentration in the deep boxes are important for both the ocean and the sediment model component. After parameter tuning, the preindustrial deep-sea $[CO_3^{2-}]$ as predicted by LOSCAR and calculated based on GLODAP data (Key et al., 2004) are in good agreement (Fig. 5). The preindustrial inventory of $CaCO_3$ in the seafloor-bioturbated sediment layer (in units of carbon) is about 800 Pg C, close to the value of more complex models (e.g. Archer et al., 1998).

In summary, after model-data comparison including all variables shown in Fig. 5, the values for the parameters labeled "tuned" in Table 2 were obtained. The preindustrial (steady-state) $p\mathrm{CO}_2$ in the model was set to 280 µatm by assigning this value to $p\mathrm{CO}_2^0$, which drives the system towards the desired steady-state $p\mathrm{CO}_2$ via the silicate weathering equation (Eq. 17). Regarding the Paleocene/Eocene model setup, several key parameters such as deep-sea $[CO_3^{2-}]$ and the calcite compensation depth (CCD) before and during the PETM have been discussed elsewhere and are not repeated here (see Zeebe et al., 2009, Supplementary Information). In the default LOSCAR setup, the CCD is taken as the depth at which the $CaCO_3$ sediment content is reduced to 10 wt. % (Ridgwell and Zeebe, 2005). The pre-PETM inventory of $CaCO_3$ in the seafloor-bioturbated sediment layer (in units of carbon) is about 620 Pg C. The initial (steady-state) partial pressure of atmospheric CO_2 was set to 1000 µatm in our P/E-simulations. Although this value falls within the (large) range of available proxy estimates, it is somewhat arbitrary. The user is welcome to change the initial $p\mathrm{CO}_2$ value in the P/E-setup.

9 Input/output examples

In the following, two input/output examples will be presented, one dealing with anthropogenic fossil fuel emissions, the other with carbon release during the PETM. The input files for these examples are included in the model package.

9.1 Fossil fuel emission scenario

LOSCAR can read in files that supply a time series of fossil fuel emissions in order to project future changes in atmospheric CO_2, surface ocean pH, calcite and aragonite saturation, and other variables (cf. Zeebe et al., 2008, Supporting Online Material). For example, Fig. 6 shows results obtained with LOSCAR for a fossil fuel emission scenario with a total carbon release of 1000 Pg C over 500 yr. Note that the results differ slightly from those in Zeebe et al. (2008) because ocean temperature was held constant here for simplicity. The initial conditions from which the scenario was started are the preindustrial steady-state conditions shown in Fig. 5. No changes in the biological pump were assumed (PO_4 is constant). The temperature of the low- and high-latitude box is 20 and 2 °C, respectively (Table 2). This temperature difference is mostly responsible for the difference in carbonate ion concentration ($[CO_3^{2-}]$) and saturation state (Ω) between low- and high-latitude surface boxes. Note that

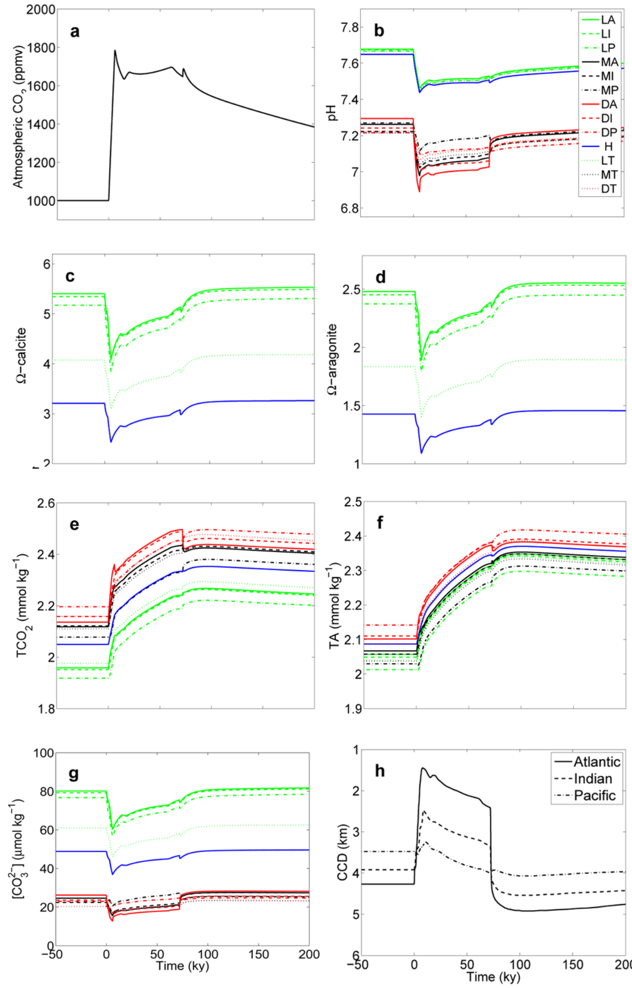

Fig. 7. Example of a PETM carbon release scenario simulated in LOSCAR: initial release of 3000 Pg C over a few thousand years (see Zeebe et al., 2009). L = Low-latitude, M = interMediate, D = Deep, H = High-latitude. A = Atlantic, I = Indian, P = Pacific, T = Tethys. See text for details.

while TCO_2 in the surface boxes responds immediately to the fossil fuel carbon release, there is a delay in TA, which only starts rising once sediment dissolution commences and the calcite compensation depth (CCD) starts shallowing (cf. Ilyina et al., 2009).

9.2 Paleocene-Eocene Thermal Maximum

Using appropriate boundary conditions, LOSCAR can also be used to simulate time intervals or events of the past such as the PETM. During the PETM, a large mass of carbon was released into Earth's surface reservoirs (e.g. Dickens et al., 1995; Zachos et al., 2005; Dickens, 2011), while surface temperatures rose by 5–9 °C within a few thousand years. Figure 7 shows results for a PETM scenario with an initial carbon input of 3000 Pg C over a few thousand years, which yields close agreement with observations (for more details, see Zeebe et al., 2009). Note that the time interval of the integration now covers 200 kyr ($t = 0$ refers to the P/E boundary), rather than a few millennia as in the previous example. Changes in boundary conditions compared to the modern setup include a Paleocene/Eocene bathymetry (Bice and Marotzke, 2002), addition of the Tethys ocean, and different seawater chemistry (see Sect. 7.2). Furthermore, the PETM simulations use different initial conditions for e.g. temperature, steady-state $p\mathrm{CO}_2^0$, weathering fluxes (Tables 2 and 3), and different steady-state circulation patterns (see Fig. 2). Note also that a transient contribution of North Pacific Deep Water (not shown) during the PETM main phase was included in our simulations (Bice and Marotzke, 2002; Zeebe et al., 2009). The Southern Ocean source remains active during the event but is reduced relative to its pre-event strength (down to 7.5 Sv). The transport associated with the North Pacific source is 6.25 Sv. This overall reduced global overturning circulation during the PETM main phase is consistent with a sluggish circulation found in a fully coupled atmosphere-ocean general circulation model with Eocene boundary conditions at high atmospheric CO_2 concentrations (Lunt et al., 2010).

At steady-state $p\mathrm{CO}_2^0$ of 1000 µatm, but similar carbonate mineral saturation state as in the modern ocean, the steady-state pH of the Paleocene/Eocene ocean would have been lower than modern (Fig. 7). Because of higher seawater Ca^{2+} and the effect of Mg/Ca on the solubility product of calcite, the initial carbonate ion concentration in the P/E-simulations is substantially lower than in the modern ocean (cf. Sect. 7.2). As a result, steady-state TCO_2 and TA are similar to modern values despite higher $p\mathrm{CO}_2$ (Fig. 7). Note that the Atlantic CCD shoals dramatically during the event, while there is little response in the Pacific CCD, consistent with observations (Zachos et al., 2005; Zeebe et al., 2009; Leon-Rodriguez and Dickens, 2010). The "overshoot" of the CCD, i.e. the fact that its position is deeper at $t > 80$ kyr than its initial position, is a direct consequence of the weathering feedback (see Sect. 4) and is also in agreement with observations (e.g. Kelly et al., 2005). At $t > 80$ kyr, atmospheric $p\mathrm{CO}_2$ is still elevated over the initial $p\mathrm{CO}_2^0$ (Fig. 7), which causes enhanced weathering of carbonates and silicates. The enhanced weathering raises the ocean's saturation state and deepens the CCD until a quasi steady-state of riverine flux and burial has been established. The quasi steady-state ($t > 80$ kyr) must be maintained at a CCD deeper than the initial depth (because of enhanced burial) until atmospheric $p\mathrm{CO}_2$ and weathering fluxes have returned to their initial steady-state values. This explains the "overshoot" of the CCD.

10 Model intercomparison: lifetime of fossil fuel CO_2

Several carbon cycle processes as simulated in LOSCAR can be quantitatively compared to other models by examining the numerical results. For instance, Archer et al. (2009) conducted a model intercomparison focusing on the long tail of the lifetime of fossil fuel CO_2. The results of that study allow comparison of carbon cycle dynamics between models, including processes such as ocean uptake of fossil fuel CO_2, reaction of CO_2 with deep-sea sediment $CaCO_3$, and the long-term effects of weathering on fossil fuel neutralization. The model intercomparison included two experiments in which pulses of 1000 and 5000 Pg C were added to the models' atmospheres and the subsequent model response was followed over 10 000 yr. For each of the pulses, the effects of various feedbacks were tested, including changes in temperature/climate, sediment response, and weathering.

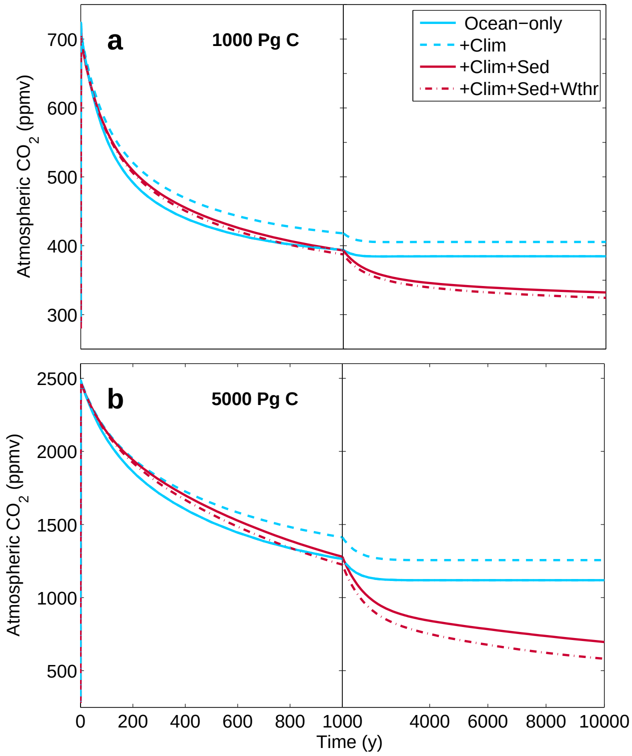

Fig. 8. LOSCAR simulations of the long tail of the lifetime of fossil fuel CO_2 (cf. Archer et al., 2009). **(a)** Simulated atmospheric CO_2 concentrations in response to a 1000 Pg C pulse, **(b)** 5000 Pg C pulse. "Ocean-only" runs include ocean CO_2 uptake only (sediments off, weathering feedback off). "+Clim" runs include an additional temperature feedback of 3 °C per CO_2 doubling (see Sect. 7.3). "+Clim+Sed" runs include the temperature and sediment feedback (weathering fluxes are held constant). "+Clim+Sed+Wthr" runs include the temperature, sediment, and weathering feedback.

The results of the corresponding model experiments with LOSCAR are shown in Fig. 8. Generally, the atmospheric CO_2 levels over time as calculated with LOSCAR fall in the lower to mid range of the atmospheric CO_2 levels calculated with the nine models compared by Archer et al. (2009).

LOSCAR's equilibration time (τ) for ocean uptake was obtained by fitting an exponential, $\propto e^{-t/\tau}$, to the model $p\mathrm{CO_2}$ over the first few hundred years for the ocean-only case (no changes in climate, sediments off, weathering off). This yields values for τ of 216 yr and 500 yr for the 1000 and 5000 Pg C pulse, respectively. The corresponding average of all models studied by Archer et al. (2009) is 250 yr and 450 yr, respectively. When a temperature feedback of 3°C per CO_2 doubling is included in LOSCAR (see Sect. 7.3), τ for ocean uptake increases to 267 yr and 595 yr for the 1000 and 5000 Pg C pulse, respectively. In LOSCAR, the increased equilibration time for ocean CO_2 uptake is solely due to higher ocean temperature, which reduces the solubility of CO_2 and leaves a larger fraction of CO_2 in the atmosphere. Some of the models analyzed by Archer et al. (2009) show larger effects of climate change on ocean uptake, presumably due to additional changes in ocean circulation and mixing.

The next step in the process of fossil fuel neutralization after ocean uptake is reaction of CO_2 with carbonate sediments in the deep sea, promoting $CaCO_3$ dissolution. In LOSCAR, it takes several millennia for the carbonate content in deep-sea sediments to reach its minimum. In contrast to ocean uptake, however, an exponential is a poor fit to the model's $p\mathrm{CO_2}$ decline during the time interval of carbonate dissolution. Nevertheless, in the time window from 1000 to 3000 yr, and exponential fit yields an approximate response time of ~ 4200 yr and ~ 3800 yr for the 1000 and 5000 Pg C pulse, respectively. For comparison, the $CaCO_3$ response time scale of the models tested by Archer et al. (2009) varies roughly between 3000 and 8000 yr. The final step of fossil fuel neutralization is enhanced weathering of carbonate and silicate rocks on the continents, which restores $p\mathrm{CO_2}$ to its long-term steady-state value (see Sect. 4). Note that constant carbonate and silicate weathering fluxes are also included in the LOSCAR experiments labeled "+Sed" in Fig. 8. However, experiments labeled "+Wthr" include a weathering feedback with enhanced weathering fluxes at elevated $p\mathrm{CO_2}$. On a time scale of 10^4 yr, the effect on fossil fuel neutralization from the addition of the weathering feedback is smaller than that from the addition of sediments (Fig. 8). This is consistent with the results of Archer et al. (2009). However, on time scales $> 10^5$ yr, the silicate weathering feedback becomes the dominant effect. Unfortunately, the parameters that determine the strength of the weathering feedback are not well constrained, which can lead to significant differences in calculated atmospheric CO_2 levels on time scales $> 10^5$ yr (e.g. Uchikawa and Zeebe, 2008)

In addition to simple carbon input experiments, one may also compare the average ocean CO_2 uptake between models from 1990 to 2000 using historical fossil fuel emissions. The observed uptake during the 1990s was 2.2 ± 0.4 Pg C yr^{-1} (IPCC, 2007). With a few exceptions, the models included in the intercomparison by Archer et al. (2009) cluster around 2.0 Pg C yr^{-1}; LOSCAR's value is 1.9 Pg C yr^{-1}. The bottom line is that in terms of ocean CO_2 uptake, a number of carbon cycle models – including LOSCAR – behave quite similar. This is not too surprising, given that ocean CO_2 uptake is, to a large degree, controlled by seawater carbonate chemistry, which is well known. In addition, calibration of the models is aided by the availability of a tuning target, namely, the observed ocean uptake. The sediment response among different models is more difficult to gauge due to several factors including different sediment model formulations, uncertainties in dissolution rate parameters (e.g. Morse and Mackenzie, 1990), and lack of a suitable tuning target based on observations. Nevertheless, all models tested in Archer et al. (2009) and LOSCAR agree that fossil fuel CO_2 neutralization via reaction with sedimentary $CaCO_3$ will take several millennia. Towards the end of the long tail of the CO_2 lifetime, carbon will be slowly removed from the atmosphere by enhanced silicate weathering. However, it will likely take tens to hundreds of thousands of years until $p\mathrm{CO_2}$ will return to climatically relevant levels of, say, 400 µatm in the future.

11 Model limitations and future developments

As mentioned above, LOSCAR is designed to compute the partitioning of carbon between ocean, atmosphere, and sediments on time scales ranging from centuries to millions of years. LOSCAR is not designed to address carbon cycle problems on time scales much shorter than centuries. LOSCAR is also not suitable for tackling problems that require fine horizontal and/or vertical resolution. For instance, attempting to model the interannual variability of air-sea CO_2 exchange in the Weddell Sea with LOSCAR would obviously be silly. On the other hand, LOSCAR does a reasonable job, for example, in calculating the globally averaged ocean CO_2 uptake over the decade from 1990 to 2000 (see Sect. 10). At present, LOSCAR includes one generic high-latitude box and does not explicitly resolve differences, for instance, between deep water formation sites in the North Atlantic and the Southern Ocean. As a result of this and the current modern ocean configuration in LOSCAR, water mass boundaries, say, between North Atlantic Deep Water and Antarctic Bottom Water are not being resolved. However, given LOSCAR's flexible ocean configuration, additional ocean boxes may be included to accommodate such features. In general, LOSCAR's components are designed to efficiently compute global carbon cycle dynamics. This philosophy also applies to the sediment model, which calculates changes in %$CaCO_3$ at low computational costs. On the contrary, if the goal is to model, for example, the detailed effects of organic carbon and methane oxidation on sediment pore water profiles, a different tool is required (e.g. Zeebe, 2007).

Future versions of LOSCAR may include new features such as additional boxes and tracers such as radiocarbon. Because a meaningful ^{14}C model-data comparison generally requires multiple high-latitude surface boxes, radiocarbon should be included after at least one more high-latitude surface box has been added. Other future changes may include addition of respiratory-driven carbonate dissolution in sediments. Respiratory dissolution could be important, for instance, for the steady-state position of the lysocline. However, respiratory dissolution is unlikely to have a significant effect on the evolution of sediment $\%CaCO_3$ during massive dissolution events such as those caused by large carbon inputs from e.g. fossil-fuel burning or during the PETM. Because these events have hitherto been the modeling targets for our LOSCAR applications, respiratory dissolution has not been included. Future versions of LOSCAR should consider this feature when processes are modeled for which respiratory dissolution is critical. Finally, I emphasize that LOSCAR's strength is its simplicity and efficiency, which will remain a priority in future developments. For the potential user this could mean that a different model needs to be considered altogether, if LOSCAR does not suit the problem at hand.

12 Summary

LOSCAR is a useful tool to tackle carbon cycle problems on various time scales as demonstrated in earlier applications that dealt with future projections of ocean chemistry and weathering, pCO_2 sensitivity to carbon cycle perturbations throughout the Cenozoic, and carbon/calcium cycling during the PETM (Zeebe et al., 2008; Zachos et al., 2008; Zeebe et al., 2009; Uchikawa and Zeebe, 2008; Stuecker and Zeebe, 2010; Uchikawa and Zeebe, 2010; Komar and Zeebe, 2011; Zeebe and Ridgwell, 2011; Zeebe, 2012). The present contribution has provided a coherent description of the LOSCAR model. The description will hopefully be beneficial to the readership of the journal, as well as users of the model. I anticipate that future applications will reveal the full spectrum of problems suitable to be studied with LOSCAR. The LOSCAR source code in C can be obtained from the author by sending a request to loscar.model@gmail.com.

Acknowledgements. I thank Guy Munhoven and Gary Shaffer (reviewers), and Andy Ridgwell (tachyonic editor) for their comments, which have improved the ms. Jim Zachos was instrumental in sparking my interest in the PETM, which prompted part of LOSCAR's model development. C. Chun and M. Zeebe provided insight into the KATJES algorithm. I also thank Karen Bice for providing the P/E-bathymetry.

Edited by: A. Ridgwell

References

Archer, D. E.: An atlas of the distribution of calcium carbonate in sediments of the deep sea, Global Biogeochem. Cy., 10, 159–174, 10.1029/95GB03016, 1996.

Archer, D. E.: Fate of fossil fuel CO_2 in geologic time, J. Geophys. Res., 110, 1012, C09S05, doi:10.1029/2004JC002625, 2005.

Archer, D. E., Kheshgi, H., and Maier-Reimer, E.: Dynamics of fossil fuel CO_2 neutralization by marine $CaCO_3$, Global Biogeochem. Cy., 12, 259–276, 1998.

Archer, D. E., Eby, M., Brovkin, V., Ridgwell, A., Cao, L., Mikolajewicz, U., Caldeira, K., Matsumoto, K., Munhoven, G., Montenegro, A., and Tokos, K.: Atmospheric lifetime of fossil fuel carbon dioxide, Ann. Rev. Earth Planet. Sci., 37, 117–134, doi:10.1146/annurev.earth.031208.100206, 2009.

Ben-Yaakov, S. and Goldhaber, M. B.: The influence of sea water composition on the apparent constants of the carbonate system, Deep-Sea Res., 20, 87–99, 1973.

Berner, R. A., Lasaga, A. C., and Garrels, R. M.: The carbonate-silicate geochemical cycle and its effect on atmospheric carbon dioxide over the past 100 million years, Am. J. Sci., 283, 641–683, 1983.

Bice, K. L. and Marotzke, J.: Could changing ocean circulation have destabilized methane hydrate at the Paleocene/Eocene boundary?, Paleoceanography, 17, 1018, doi:10.1029/2001PA000678 , 2002.

Broecker, W. S. and Peng, T.-H.: The role of $CaCO_3$ compensation in the glacial to interglacial atmospheric CO_2 change, Global Biogeochem. Cy., 1, 15–29, 1987.

Broecker, W. S. and Peng, T.-H.: Greenhouse Puzzles: Keelings's World, Martin's World, Walker's World, 2nd Edn., Eldigio Press, Palisades, New York, 1998.

Broecker, W. S. and Takahashi, T.: Neutralization of fossil fuel CO_2 by marine calcium carbonate, in: The Fate of Fossil Fuel CO_2 in the Oceans, edited by: Anderson, N. R. and Malahoff, A., Plenum Press, New York, 213–241, 1977.

deMenocal, P. B., Ruddiman, W. F., and Pokras, E. M.: Influences of high- and low-latitude processes on African climate: Pleistocene eolian records from equatorial Atlantic Ocean Drilling Program Site 663, Paleoceanography, 8, 209–242, 1993.

Dickens, G. R.: Down the Rabbit Hole: toward appropriate discussion of methane release from gas hydrate systems during the Paleocene-Eocene thermal maximum and other past hyperthermal events, Clim. Past, 7, 831–846, doi:10.5194/cp-7-831-2011, 2011.

Dickens, G. R., O'Neil, J. R., Rea, D. K., and Owen, R. M.: Dissociation of oceanic methane hydrate as a cause of the carbon isotope excursion at the end of the Paleocene, Paleoceanography, 10, 965–971, 1995.

Feely, R. A., Sabine, C. L., Lee, K., Millero, F. J., Lamb, M. F., Greeley, D., Bullister, J. L., Key, R. M., Peng, T.-H., Kozyr, A., Ono, T., and Wong, C. S.: In situ calcium carbonate dissolution in the Pacific Ocean, Global Biogeochem. Cy., 16, 1144, doi:10.1029/2002GB001866, 2002.

Follows, M. J., Ito, T., and Dutkiewicz, S.: On the solution of the carbonate chemistry system in ocean biogeochemistry models, Ocean Model., 12, 290–301, doi:10.1016/j.ocemod.2005.05.004, 2006.

Francey, R. J., Allison, C. E., Etheridge, D. M., Trudinger, C. M., Enting, I. G., Leuenberger, M., Langenfelds, R. L., Michel, E., and Steele, L. P.: A 1000-year high precision record of δ^{13}C in atmospheric CO_2, Tellus, 51B, 170–193, 1999.

Hayes, J. M.: Factors controlling ^{13}C contents of sedimentary organic compounds: Principles and evidence, Mar. Geol., 113, 111–125, 1993.

Herbert, T. D. and Mayer, L. A.: Long climatic time series from sediment physical property measurements, J. Sed. Petrol., 61, 1089–1108, 1991.

Ilyina, T., Zeebe, R. E., Maier-Reimer, E., and Heinze, C.: Early detection of ocean acidification effects on marine calcification, Global Biogeochem. Cy., 23, GB1008, doi:10.1029/2008GB003278, 2009.

IPCC: Intergovernmental Panel on Climate Change, Climate Change 2007: The Physical Science Basis, edited by: Solomon, S., Qin, D., Manning, M., Chen, Z., Marquis, M., Averyt, K. B., Tignor, M., and Miller, H. L., Cambridge University Press, Cambridge, 996 pp., 2007.

Keir, R.: Dissolution of calcite in the deep sea: Theoretical predictions for the case of uniform size particles settling into a well-mixed sediment, Am. J. Sci., 282, 193–236, 1982.

Keir, R. S.: On the late Pleistocene ocean geochemistry and circulation, Paleoceanography, 3, 413–445, doi:10.1029/PA003i004p00413, 1988.

Kelly, D. C., Zachos, J. C., Bralower, T. J., and Schellenberg, S. A.: Enhanced terrestrial weathering/runoff and surface-ocean carbonate production during the recovery stages of the Paleocene-Eocene Thermal Maximum, Paleoceanography, 20, PA4023 doi:10.1029/2005PA001163, 2005.

Key, R. M., Kozyr, A., Sabine, C. L., Lee, K., Wanninkhof, R., Bullister, J., Feely, R. A., Millero, F., Mordy, C., and Peng, T.-H.: A global ocean carbon climatology: Results from GLODAP, Global Biogeochem. Cy., 18, GB4031, doi:10.1029/2004GB002247, 2004.

Köhler, P., Fischer, H., and Zeebe, R. E.: Quantitative interpretation of atmospheric carbon records over the last glacial termination, Global Biogeochem. Cy., 19, GB4020, doi:10.1029/2004GB002345, 2005.

Komar, N. and Zeebe, R. E.: Changes in oceanic calcium from enhanced weathering did not affect calcium-based proxies during the Paleocene-Eocene Thermal Maximum, Paleoceanography, 26, doi:10.1029/2010PA001979, 2011.

Kroopnick, P. M.: The distribution of ^{13}C of ΣCO_2 in the world oceans, Deep-Sea Res. I, 32, 57–84, 1985.

Leon-Rodriguez, L. and Dickens, G. R.: Constraints on ocean acidification associated with rapid and massive carbon injections: The early Paleogene record at ocean drilling program site 1215, equatorial Pacific Ocean, Palaeogeogr., Palaeoclimatol., Palaeoecol., 298, 409–420, 2010.

Lueker, T. J., Dickson, A. G., and Keeling, C. D.: Ocean $p$$CO_2$ calculated from dissolved inorganic carbon, alkalinity, and equations for K_1 and K_2: validation based on laboratory measurements of CO_2 in gas and seawater at equilibrium, Mar. Chem., 70, 105–119, 2000.

Lunt, D. J., Valdes, P. J., Dunkley-Jones, T., Ridgwell, A., Haywood, A. M., Schmidt, D. N., Marsh, R., and Maslin, M.: CO_2-driven ocean circulation changes as an amplifier of Paleocene-Eocene Thermal Maximum hydrate destabilization, Geology, 38, 875–878, doi:10.1130/G31184.1, 2010.

Mayer, L. A.: Extraction of high-resolution carbonate data for palaeoclimate reconstruction, Nature, 352, 148–150, 1991.

Menard, H. W. and Smith, S. M.: Hypsometry of Ocean Basin Provinces, J. Geophys. Res., 71, 4305–4325, 1966.

Millero, F. J.: Thermodynamics of the carbon dioxide system in the oceans, Geochim. Cosmochim. Acta, 59, 661–677, 1995.

Milliman, J. D., Troy, P. J., Balch, W. M., Adams, A. K., Li, Y.-H., and Mackenzie, F. T.: Biologically mediated dissolution of calcium carbonate above the chemical lysocline?, Deep-Sea Res. I, 46, 1653–1669, 1999.

Mook, W. G.: ^{13}C in atmospheric CO_2, Netherlands Journal of Sea Research, 20, 211–223, 1986.

Morse, J. W. and Mackenzie, F. T.: Geochemistry of Sedimentary Carbonates, Developments in sedimentology, 48, Elsevier, Amsterdam, 707 pp., 1990.

Mucci, A.: The solubility of calcite and aragonite in seawater at various salinities, temperatures, and one atmosphere total pressure, Am. J. Sci., 283, 780–799, 1983.

Mucci, A. and Morse, J. W.: The solubility of calcite in seawater solutions of various magnesium concentration, $I_t = 0.697$ m at 25degC and one atmosphere total pressure, Geochim. Cosmochim. Acta, 48, 815–822, doi:10.1016/0016-7037(84)90103-0, 1984.

Munhoven, G. and Francois, L. M.: Glacial-interglacial variability of atmospheric CO_2 due to changing continental silicate rock weathering: A model study, J. Geophys. Res., 101, 21423–21437, 1996.

Opdyke, B. N. and Walker, J. C. G.: Return of the coral reef hypothesis: Basin to shelf partitioning of $CaCO_3$ and its effect on atmospheric CO_2, Geology, 20, 733–736, doi:10.1130/0091-7613(1992)020<0733:ROTCRH>2.3.CO;2, 1992.

Peacock, S., Lane, E., and Restrepo, J. M.: A possible sequence of events for the generalized glacial-interglacial cycle, Global Biogeochem. Cy., 20, GB2010, doi:10.1029/2005GB002448, 2006.

Press, W. H., Flannery, B. P., Teukolsky, S. A., and Vetterling, W. T.: Numerical Recipes in C: The Art of Scientific Computing, Cambridge University, Cambridge, 1020 pp., 1992.

Ridgwell, A. J.: Glacial-interglacial perturbations in the global carbon cycle, Ph.D. thesis, Univ. of East Anglia at Norwich, UK, 2001.

Ridgwell, A. J. and Zeebe, R. E.: The role of the global carbonate cycle in the regulation and evolution of the Earth system, Earth Planet. Sci. Lett., 234, 299–315, 2005.

Sarmiento, J. L. and Toggweiler, J. R.: A new mode of the role of the oceans in determining atmospheric P_{CO_2}, Nature, 308, 621–624, 1984.

Shaffer, G., Malskær Olsen, S., and Pepke Pedersen, J. O.: Presentation, calibration and validation of the low-order, DCESS Earth System Model (Version 1), Geosci. Model Dev., 1, 17–51, doi:10.5194/gmd-1-17-2008, 2008.

Siegenthaler, U. and Münnich, K. O.: ^{13}C/^{12}C fractionation during CO_2 transfer from air to sea, in: SCOPE 16 – The Global Carbon Cycle, edited by: Bolin, B., 249–257, Wiley & Sons, New York, 1981.

Siegenthaler, U. and Wenk, T.: Rapid atmospheric CO_2 variations and ocean circulation, Nature, 308, 624–626, 1984.

Sigman, D. M., McCorkle, D. C., and Martin, W. R.: The calcite lysocline as a constraint on glacial/interglacial low-latitude production changes, Global Biogeochem. Cy., 12, 409–427, 1998.

Stephens, B. B. and Keeling, R. P.: The influence of Antarctic sea ice on glacial-interglacial CO_2 variations, Nature, 404, 171–174, 2000.

Stuecker, M. F. and Zeebe, R. E.: Ocean chemistry and atmospheric CO_2 sensitivity to carbon perturbations throughout the Cenozoic, Geophys. Res. Lett., 37, L03609, doi:10.1029/2009GL041436, 2010.

Sundquist, E. T.: Geologic Analogs: Their value and limitations in carbon dioxide research, in: The Changing Carbon cycle: A Global Analysis, edited by: Trabalka, J. R. and Reichle, D. E., Springer-Verlag, New York, 371–402, 1986.

Thomas, D. J., Bralower, T. J., and Jones, C. E.: Neodymium isotopic reconstruction of late Paleocene-early Eocene thermohaline circulation, Earth Planet Sci. Lett., 209, 309–322, 2003.

Toggweiler, J. R.: Variation of atmospheric CO_2 by ventilation of the ocean's deepest water, Paleoceanography, 14, 571–588, 1999.

Tyrrell, T. and Zeebe, R. E.: History of carbonate ion concentration over the last 100 million years, Geochim. Cosmochim. Acta, 68, 3521–3530, 2004.

Uchikawa, J. and Zeebe, R. E.: Influence of terrestial weathering on ocean acidification and the next glacial inception, Geophys. Res. Lett., 35, L23608, doi:10.1029/2008GL035963, 2008.

Uchikawa, J. and Zeebe, R. E.: Examining possible effects of seawater pH decline on foraminiferal stable isotopes during the Paleocene-Eocene Thermal Maximum, Paleoceanography, 25, PA2216, doi:10.1029/2009PA001864, 2010.

Walker, J. C. G. and Kasting, J. F.: Effects of fuel and forest conservation on future levels of atmospheric carbon dioxide, Palaeogeogr. Palaeoclim. Palaeoecol., 97, 151–189, 1992.

Walker, J. C. G., Hays, P. B., and Kasting, J. F.: Negative feedback mechanism for the long-term stabilization of earth's surface temperature, J. Geophys. Res., 86, 9776–9782, 1981.

Wanninkhof, R.: Kinetic fractionation of the carbon isotopes ^{13}C and ^{12}C during transfer of CO_2 from air to seawater, Tellus, 37B, 128–135, 1985.

WOA05: World Ocean Atlas 2005, NOAA Atlas NESDIS 61, Washington, DC, available at: http://www.nodc.noaa.gov/OC5/WOA05/pr_woa05.html (last access: 21 January 2012), 2005.

Zachos, J. C., Röhl, U., S. A. Schellenberg, A. S., Hodell, D. A., Kelly, D. C., Thomas, E., M. Nicolo, I. R., Lourens, L. J., McCarren, H., and Kroon, D.: Rapid acidification of the ocean during the Paleocene-Eocene Thermal Maximum, Science, 308, 1611–1615, 2005.

Zachos, J. C., Dickens, G. R., and Zeebe, R. E.: An early Cenozoic perspective on greenhouse warming and carbon-cycle dynamics, Nature, 451, 279–283, doi:10.1038/nature06588, 2008.

Zeebe, R. E.: Modeling CO_2 chemistry, $\delta^{13}C$, and oxidation of organic carbon and methane in sediment porewater: Implications for paleo-proxies in benthic foraminifera, Geochim. Cosmochim. Acta, 71, 3238–3256, 2007.

Zeebe, R. E.: Where are you heading Earth? (Commentary), Nat. Geosci., 4, 416–417, 2011.

Zeebe, R. E.: History of seawater carbonate chemistry, atmospheric CO_2, and ocean acidification, Annu. Rev. Earth Planet. Sci, 40, 141–165, doi:10.1146/annurev-earth-042711-105521, 2012.

Zeebe, R. E. and Caldeira, K.: Close mass balance of long-term carbon fluxes from ice-core CO_2 and ocean chemistry records, Nat. Geosci., 1, 312–315, doi:10.1038/ngeo185, 2008.

Zeebe, R. E. and Ridgwell, A.: Past changes of ocean carbonate chemistry, in: Ocean Acidification, edited by: Gattuso, J.-P. and Hansson, L., Oxford University Press, 2011.

Zeebe, R. E. and Westbroek, P.: A simple model for the $CaCO_3$ saturation state of the ocean: The "Strangelove", the "Neritan", and the "Cretan" Ocean, Geochem. Geophys. Geosyst., 4, 1104, doi:10.1029/2003GC000538, 2003.

Zeebe, R. E. and Wolf-Gladrow, D. A.: CO_2 in Seawater: Equilibrium, Kinetics, Isotopes, Elsevier Oceanography Series, Amsterdam, 346 pp., 2001.

Zeebe, R. E. and Zachos, J. C.: Reversed deep-sea carbonate ion basin-gradient during Paleocene-Eocene Thermal Maximum, Paleoceanography, 22, PA3201, doi:10.1029/2006PA001395, 2007.

Zeebe, R. E., Zachos, J. C., Caldeira, K., and Tyrrell, T.: Oceans: Carbon Emissions and Acidification (in Perspectives), Science, 321, 51–52, doi:10.1126/science.1159124, 2008.

Zeebe, R. E., Zachos, J. C., and Dickens, G. R.: Carbon dioxide forcing alone insufficient to explain Palaeocene-Eocene Thermal Maximum warming, Nat. Geosci., 2, 576–580, doi:10.1038/ngeo578, 2009.

Zhang, J., Quay, P. D., and Wilbur, D. O.: Carbon isotope fractionation during gas-water exchange and dissolution of CO_2, Geochim. Cosmochim. Acta, 59, 107–114, 1995.